

Electronic Thesis and Dissertation Repository

1-15-2016 12:00 AM

Examining the role of ATRX in astrocytes

Haley McConkey

The University of Western Ontario

Supervisor

Dr. Nathalie Berube

The University of Western Ontario

Graduate Program in Biochemistry

A thesis submitted in partial fulfillment of the requirements for the degree in Master of Science

© Haley McConkey 2016

Follow this and additional works at: <https://ir.lib.uwo.ca/etd>



Part of the [Biochemistry Commons](#), and the [Molecular and Cellular Neuroscience Commons](#)

Recommended Citation

McConkey, Haley, "Examining the role of ATRX in astrocytes" (2016). *Electronic Thesis and Dissertation Repository*. 3502.

<https://ir.lib.uwo.ca/etd/3502>

This Dissertation/Thesis is brought to you for free and open access by Scholarship@Western. It has been accepted for inclusion in Electronic Thesis and Dissertation Repository by an authorized administrator of Scholarship@Western. For more information, please contact wlsadmin@uwo.ca.

Abstract

Astrocytes perform many homeostatic roles in the brain while supplying metabolites to neurons and mediating synaptic transmission. The current study explored a possible role of the *Atrx* gene in astrocytes. Hypomorphic mutations in this gene cause the ATR-X intellectual disability syndrome. Deletion of *Atrx* in the forebrain leads to an apparent increase in reactive astrocytes, potentially caused by the high level of neuroprogenitor cell death. To avoid such non cell-autonomous effects on astrocytes, we generated mice with inducible conditional inactivation of *Atrx* in astrocytes. Preliminary analysis two weeks following induction of *Atrx* gene deletion revealed variably lower expression of *Connexin 30 (Gjb6)*, encoding a gap junction protein. Morphologically, ATRX-null astrocytes displayed larger domain coverage by peripheral astrocytic processes, suggesting altered functionality. This work provides key advances to our understanding of ATRX function in astrocytes and provides a unique mouse model for future investigations.

Keywords

ATRX, *Alpha thalassemia mental retardation*, *X-linked*, astrocytes, astrocyte morphology, inducible gene deletion

Co-Authorship Statement

I participated in the design and execution of all experiments, performed data analysis, and prepared all written material, with the following exceptions:

In Chapter 3.1, P7 cryosections from *Foxg1* control and conditional knockout males were obtained by Dr. Kieran Richie. Protein extracts and cryosections from P20 *Foxg1* control and conditional knockout males were obtained by Matt Edwards.

In Chapter 3.3, RNA extractions from P26 control and inducible knockout male hippocampus and cortex were performed by Yan Jiang. Hippocampal and cortical qRT-PCR for P26 control and inducible knockout males was performed by Dr. Michael Levy.

Acknowledgments

I have received support and encouragement throughout my academic career from so many wonderful people. Firstly, I need to thank my family. To my Dad, thank you for always being there to listen to me complain about stressful weeks and for listening to me talk constantly, likely at a barely understandable speed, about my project. All my close friends, old and new, I need to extend my gratitude for dealing with me at my worst and making me laugh no matter what. My sanity would have been lost without you and I am forever thankful for all the kind words and gestures that have kept me going.

To my supervisor, Dr. Nathalie Bérubé, thank you for all your guidance throughout my Master's degree. Your passion for science is inspiring and it was a pleasure to be a part of your lab. To my fellow lab members, past and present, thank you for making the lab a fun place to be. I have learned so much from all of you and my time in graduate school would not have been the same without you. I would finally like to thank my advisory committee, Dr. Joe Torchia and Dr. Arthur Brown, for your invaluable advice and insight throughout my thesis project.

Table of Contents

Abstract	i
Co-Authorship Statement	ii
Acknowledgments	iii
Table of Contents	1
List of Tables	3
List of Figures	4
List of Abbreviations	6
Chapter 1	8
1 Introduction	8
1.1 Astrocytes	8
1.1.1 Functions of astrocytes in the CNS	9
1.1.2 Astrocyte development and maturation	12
1.1.3 The role of astrocytes at the synapse	13
1.1.4 Astrocyte involvement in the pathology of neurodevelopmental disorders	18
1.1.5 Alpha thalassemia mental retardation X-linked syndrome	21
1.2 ATRX is a key regulator of chromatin structure	23
1.2.1 Gene location and protein structure	23
1.2.2 ATRX's diverse functions in the cell and at chromatin	25
1.2.3 ATRX and neuronal development	27
1.3 Hypothesis and Summary of Findings	29
2 Materials and Methods	31
2.1 Animal Husbandry and Genotyping	31
2.2 Tamoxifen Preparation and Injection	33

2.3 Western Blot Analysis	38
2.4 Quantitative Real Time PCR (qRT-PCR).....	39
2.5 Immunofluorescence and Cell Counts	41
2.6 Microarray Analysis.....	42
3 Results	46
3.1 Assessing the astrocyte population in <i>Atrx^{f/y}Foxg1-Cre</i> mice	46
3.2 Creation of a novel mouse model deleting <i>Atrx</i> in astrocytes	57
3.3 Preliminary morphological assessment of ATRX-null astrocytes	67
4 Discussion	72
4.1 Loss of ATRX in the forebrain affects the astrocyte population	72
4.1.1 <i>Aldh1l1</i> expression and the number of astrocytes present in the <i>cKO</i> is variable.....	72
4.1.2 <i>ATRX</i> loss in the embryonic forebrain results in altered expression of astrocytes enriched genes.	74
4.2 Creation of a novel mouse model	76
4.3 Altered morphology and decreased expression of gap junction protein in inducible KO.....	79
4.3.1 <i>Increase in number of astrocytes undergoing recombination and altered morphology in the cortex at P26 in inducible KO</i>	79
4.3.2 <i>Change in connexin 30 (Gjb6) expression in cortex of inducible KO at P26</i>	82
Conclusions and future directions	83
References	85
Appendix A – Ethics Approval	95

List of Tables

Table 1. Overlapping symptoms of three neurodevelopmental disorders	22
Table 2. Summary of mouse genotypes used within this thesis, grouping control and knockout pairs compared by colour.	34
Table 3. List of Primers used for genotyping	37
Table 4. Primers used for qRT-PCR.....	43
Table 5. List of antibodies used for immunofluorescence (IF) and western blot (WB) experiments.....	44

List of Figures

Figure 1. Astrocytes perform many essential functions at the synapse and the blood brain barrier	10
Figure 2. Timeline of astrocyte development in the mouse	14
Figure 3. Schematic of ATRX protein	24
Figure 4. <i>LoxP</i> site placement in <i>Atrx</i> gene	35
Figure 5. Schematic representation of the <i>mT/mG</i> fluorescent reporter allele....	36
Figure 6. Regions of the mouse brain used for experimental analysis	45
Figure 7. Potential reactive astrocyte activation in cKO compared to control hippocampus at P7	47
Figure 8. Quantification of Aldh111 and GFAP proteins levels in the cKO forebrain at P20	49
Figure 9. The number of astrocytes is not changed in the cortex of P20 cKO males compared to controls	51
Figure 10. Astrocyte-enriched genes demonstrate altered transcript levels in the forebrain of cKO males at P17.....	54
Figure 11. <i>Atrx</i> expression is not significantly decreased in the hippocampus of inducible knockout males	58
Figure 12. <i>Atrx</i> expression in the cortex of P26 control and inducible KO mice .	59
Figure 13. Percent of GFAP+ nuclei lacking ATRX is significantly increased in P26 hippocampus of inducible knockout compared to control	61
Figure 14. ATRX protein expression is decreased in cerebellum of P26 cerebellum of inducible KO.....	64

Figure 15. GFP expression in the cortex and hippocampus after tamoxifen administration in male mice carrying the <i>mT/mG</i> allele	66
Figure 16. ATRX ⁻ GFP ⁺ astrocytes display altered morphology in the P26 cortex	69
Figure 17. Expression analysis of astroglial genes in the P26 cortex of control and inducible KO mice.....	71

List of Abbreviations

A	Adenine
ADD	ATRX-DNMT3-DNMT3L
Aldh1l1	Aldehyde Dehydrogenase 1 Family, Member L1
AMPA	alpha-amino-3-hydroxy-5-methyl-4-isoxazolepropionic acid receptor
Aqp4	Aquaporin 4
ATP	adenosine triphosphate
ATPase	Adenosine triphosphate synthase
ATRX	Alpha thalassemia mental retardation X-linked
ATR-X	Alpha thalassemia mental retardation, X-linked (referring to syndrome)
BSA	Bovine serum albumin
C	Cytosine
C1q	Complement Component 1, Q Subcomponent, Alpha Polypeptide
cDNA	Complementary deoxyribonucleic acid
cKO	Conditional knockout
CpG	Cytosine-guanine dinucleotide
CTCF	CCCTC-Binding Factor (Zinc Finger Protein)
DAPI	4',6-diamidino-2-phenylindole
Daxx	Death-associated protein 6
Dio2	Deiodonase-2
DNMT	DNA methyltransferase
dNTP	Deoxynucleotide
DTT	Dithiothreitol
E#	Mouse embryonic day #
ECL	Enhanced chemiluminescence
FMR1	Fragile X mental retardation 1
FMRP	Fragile X mental retardation protein
Foxg1	Forkhead Box G1
G	Guanine
Gapdh	Glyceraldehyde-3-Phosphate Dehydrogenase
GFAP	Glial fibrillary acidic protein
GFP	Enhanced green fluorescent protein
Gja1	Gap Junction Protein, Alpha 1, 43kDa (Connexin 43)
Gjb6	Gap Junction Protein, Beta 6, 30kDa (Connexin 30)
Slc1a2	Solute carrier family 1 (glial high affinity glutamate transporter), member 2
GO	Gene ontology
H3.3	Histone 3 variant 3

H3K4	Histone three, unmethylated lysine four
H3K9me3	Histone three lysine nine trimethylation
HeLa	Henrietta Lacks (cervical cancer cells)
HP1 α	Heterochromatin-associated protein 1 alpha
IGF-1	Insulin-like growth factor 1
INCENP	Inner Centromere Protein Antigens 135/155kDa
kb	Kilobase
kDa	Kilodalton
Kir4.1	Potassium channel, inwardly rectifying subfamily J, member 10
Lox	Lysyl oxidase
MeCP2	Methyl CpG binding protein 2
mGluR	Metabotropic Glutamate Receptor
mRNA	Messenger ribonucleic acid
OCT	Optimal cutting temperature compound
P#	Mouse postnatal day #
p53	Tumour suppressor protein 53
PAP	Peripheral astrocyte process
PBS	Phosphate buffered saline
PFA	Paraformaldehyde
qRT-PCR	Quantitative reverse transcription polymerase chain reaction
Rad54	DNA Repair And Recombination Protein RAD54B
RGC	Retinal ganglion cell
RIPA	Radioimmunoprecipitation assay buffer
Slc4a4	Solute Carrier Family 4 (Sodium Bicarbonate Cotransporter)
SPARC	Secreted Protein, Acidic, Cysteine-Rich
Swi/Snf	Switch/sucrose-nonfermenting
T	Thymine
TAM	Tamoxifen
TBS-T	Tris-Buffered Saline and Tween 20
TGF- β	Transforming growth factor beta
TNC	Tenascin C
TNF- β	Tumour necrosis factor beta
γ H2AX	Gamma-Histone 2A family, member X

Chapter 1

1 Introduction

1.1 Astrocytes

There are many different cell types in the brain, including neurons, and glia cells which include astrocytes, oligodendrocytes and microglia. Research on brain development and function has historically been focused on neurons and oligodendrocytes. The astrocyte is only beginning to become an area of interest and appears to have importance in normal brain function. It was estimated that between 20 to 40% of all cells in mammalian brains are astrocytes (Herculano-Houzel, 2014). The number of astrocytes does vary depending on species and area of the brain (Khakh and Sofroniew, 2015). Astrocytes are sparse in areas with numerous neuron cell bodies but are abundant in areas populated with axons and dendrites (Khakh and Sofroniew, 2015). Human astrocytes are up to 20x larger in volume and contact up to 10x more synapses compared to rodent astrocytes (Oberheim *et al.*, 2009). Important synaptic proteins produced in astrocytes are more abundant in the human brain compared to chimpanzees and macaques (Caceres *et al.*, 2007). These findings support an important role for astrocytes in the human brain.

The functional diversity of astrocytes is still underappreciated, however two distinct types of astrocytes have been identified. Protoplasmic astrocytes are found in the gray matter and surround synapses (Sofroniew and Vinters, 2010). They have

many fine branches, called peripheral astrocytic processes (or PAPs) that connect to synapses, blood vessels, and other astrocytes, and account for approximately 80% of the cell's surface area (Rossi, 2015). Fibrous astrocytes are present in the white matter and have many long fiber-like processes that make contacts with axons (Sofroniew and Vinters, 2010). GFAP (glial fibrillary acidic protein) is used to label astrocytes, but this protein labels astrocyte subtypes differently (Rossi, 2015). Fibrous astrocytes express higher levels of GFAP throughout their processes (Cahoy *et al.*, 2008; Rossi, 2015) while GFAP expression is weaker in protoplasmic astrocytes and is mainly in the cell body and immediate large processes (Cahoy *et al.*, 2008; Sofroniew and Vinters, 2010). The amount of GFAP present in astrocytes also varies in different brain regions. For example, hippocampal astrocytes express high levels whereas cortical astrocytes express low levels (Khakh and Sofroniew, 2015). GFAP is also upregulated in reactive astrogliosis (Sofroniew and Vinters, 2010), a topic that will be discussed further in the next section. There are many other differences between astrocytes, including morphology and density, depending on area of the murine brain (Emsley and Macklis, 2006; Khakh and Sofroniew, 2015).

1.1.1 Functions of astrocytes in the CNS

Astrocytes have long been regarded as support cells in the brain, as reviewed by Sofroniew and Vinters (2010) and Rossi (2015) (Figure 1). While they do perform

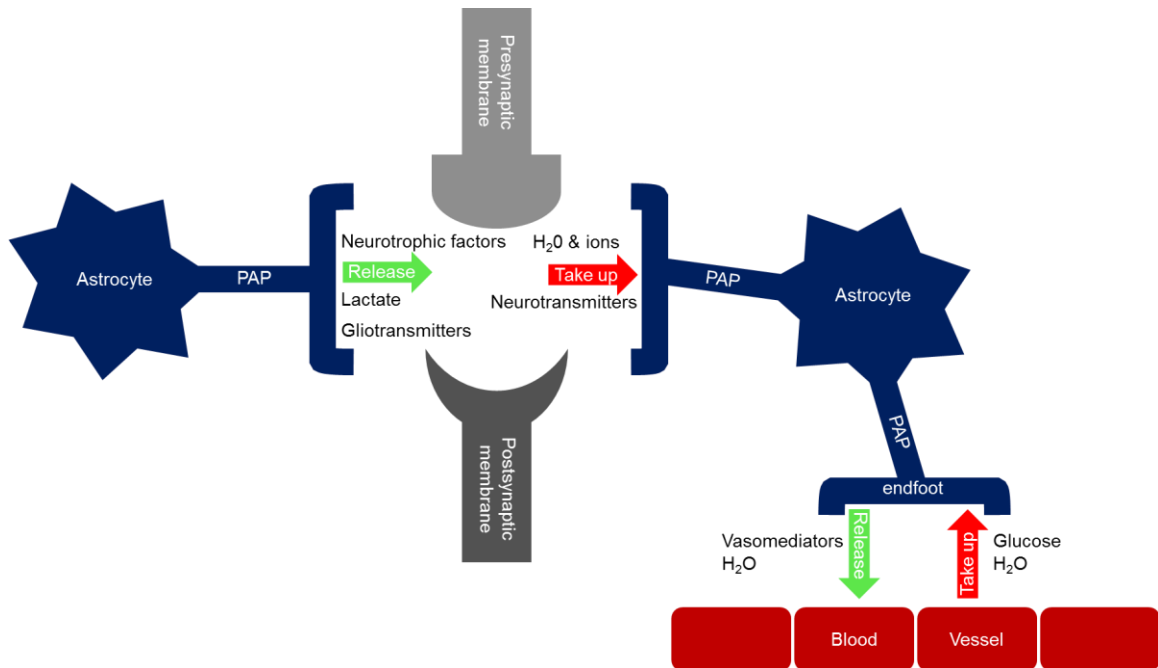


Figure 1. Astrocytes perform many essential functions at the synapse and the blood brain barrier. The astrocyte PAPs extend to make connections at the synapse and contact blood brain barrier with their endfeet. At the synapse, astrocytes release important neurotrophic factors during development to induce synapse formation. Lactate is released to neurons during periods of high neuronal activity and gliotransmitters are also released to help modulate synaptic function of neurons. Astrocytes also take up excess neurotransmitters present at the synapse. pH and ion homeostasis is maintained at the synapse through water and ion uptake by astrocytes. Astrocytes are the only cells that contact blood vessels in the brain and take up glucose and control water levels in the brain. Astrocytes can also release vasodilators to modulate blood flow based on neuronal activity and metabolic demand.

many vital functions to support neuronal homeostasis, astrocytes also have key roles in synaptic plasticity and the response to brain injury (Rossi, 2015; Sofroniew and Vinters, 2010). Astrocytes are the only cell type in the brain to make contacts with the blood vessels and can secrete factors that mediate blood flow based on neural activity (Quaeghebeur *et al.*, 2011). They are also the site of glycogen storage in the brain, with the highest amount of glycogen accumulation in astrocytes in areas of high synaptic density (Belanger *et al.*, 2011; Sofroniew and Vinters, 2010). Astrocytes also maintain fluid, ion, and pH homeostasis at the synapse (Rossi, 2015; Sofroniew and Vinters, 2010), contact blood vessels to allow for control of fluid homeostasis (Sofroniew and Vinters, 2010), and take up excess neurotransmitters from the synaptic space to prevent prolonged stimulation (Rossi, 2015; Sofroniew and Vinters, 2010). Astrocytes form a network with each other through gap junctions to allow for efficient communication and to deplete the molecules they take up and prevent accumulation of said molecules at the synapse and within a single astrocyte (Rossi, 2015; Sofroniew and Vinters, 2010).

Astrocytes are also important in responding to brain injury, cell death, and inflammation as they are capable of forming glial borders, and possibly glial scars, to contain damage from an insult (Sofroniew and Vinters, 2010). Astrocytes responding to these events are called reactive astrocytes and their characteristics include: (1) upregulation of GFAP, as well as other genes, (2) hypertrophy of the cell body and processes, and (3) proliferation (if damage is significant) to reorganize the tissue and contain inflammation (Sofroniew and Vinters, 2010). This process is also referred to as astrogliosis. Depending on the severity of the brain

injury, a glial scar may form to act as a barrier around the injury to protect surrounding tissue from inflammation (Sofroniew and Vinters, 2010).

1.1.2 Astrocyte development and maturation

Astrocytes begin to appear just before birth at approximately embryonic day 18.5, or E18.5, and peak astroglialogenesis continues until postnatal day 7, or P7, in mice (Yang *et al.*, 2013). Following the end of neurogenesis, radial glia progenitor cells switch from a neuronal to an astrocytic differentiation program (Anthony *et al.*, 2004; Yang *et al.*, 2013). New astrocytes continue to divide while differentiating to produce clonal astrocytes locally (Garcia-Marques and Lopez-Mascaraque, 2013; Ge *et al.*, 2012; Tsai *et al.*, 2012), however, astrocytes are not fully mature until 3 to 4 weeks after birth (Freeman, 2010; Yang *et al.*, 2013).

The morphological maturation of astrocytes that occurs postnatally involves the extension of PAPs. These processes are required to make contacts with other astrocytes, synapses and blood vessels (Yang *et al.*, 2013). PAPs from one astrocyte can contact approximately 100,000 synapses in the rodent brain and up to 2,000,000 in the human as astrocyte size is drastically increased (Oberheim *et al.*, 2006). These processes form between P14 and P26 (Yang *et al.*, 2013) which is also the time of peak synaptogenesis (occurring between P14 and P21) (Freeman, 2010). PAPs often overlap between astrocytes during this time of intense outgrowth, but are eventually pruned so that astrocytes occupy specific and distinct domains by 4 weeks of age (Bushong *et al.*, 2004). These astrocyte domains represent the area covered by PAPs. This morphological maturation is

followed, with brief overlap, by the induction of several astroglial genes. Glutamate transporter Slc1a2, gap junction proteins connexin 30 (Gjb6) and connexin 43 (Gja1), and potassium channel Kir.1, for example, are all induced between P21 and P28 (Yang *et al.*, 2013). This timeline (Figure 2) suggests that mature astrocyte morphology is tightly associated with molecular maturation as the astroglial genes mentioned above are all membrane proteins present at PAPs and used at the synapse (Yang *et al.*, 2013).

1.1.3 The role of astrocytes at the synapse

As astrocytes extend their processes they guide the migration of developing axons and neurons by forming molecular boundaries (Powell and Geller, 1999). Astrocytes also help refine synaptic processes by taking part in synaptic pruning (Stevens *et al.*, 2007). Stevens *et al.* reported that C1q, an initiating protein in the complement cascade (part of the innate immune system response) is upregulated in postnatal neurons in the presence of immature astrocytes. C1q was later determined to be induced by TGF- β , an astrocyte-secreted factor that initiates the complement cascade in neurons, leading to synaptic pruning in the developing visual system (Bialas and Stevens, 2013).

Astrocytes are also extremely important in synaptogenesis. A pioneering study provided evidence that synapse formation was limited without the presence of glial cells (Ullian *et al.*, 2001). The authors demonstrated that neurons cultured in the absence of astrocytes, or astrocyte-conditioned media, formed very few synapses and those that did form were functionally immature (Ullian *et al.*, 2001). Through

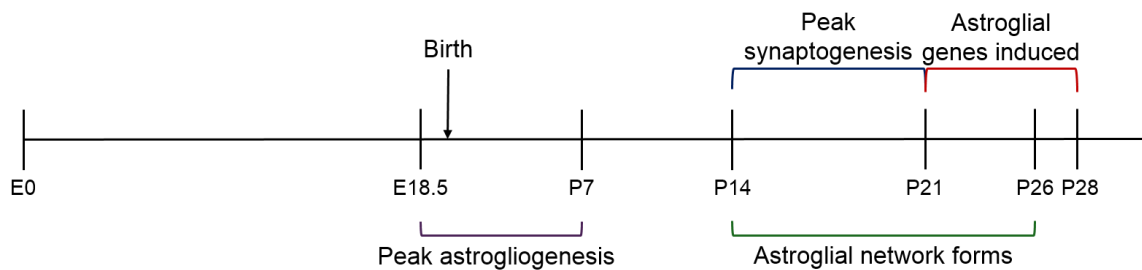


Figure 2. Timeline of astrocyte development in the mouse. Embryonic day 0 (E0) represents conception and peak astroglialogenesis, or astrocyte production, occurs shortly before birth at E18.5 and continues to approximately a week after birth (P7). The astrocytes produced are immature and do not begin to extend PAPs and form networks with each other and synapses until two weeks after birth (P14). This morphological maturation of astrocytes overlaps with peak synapse formation between neurons. Molecular maturation through expression of astroglial genes also overlaps with the end of the morphological maturation period, beginning at 3 weeks after birth (P21).

the use of electron microscopy and immunofluorescence directed at detecting synaptic proteins and astrocytic markers, they demonstrated that synapse formation corresponds with the appearance of astrocytes in the mouse brain (Ullian *et al.*, 2001).

Many astrocyte-secreted molecules were subsequently identified as important signals for synapse formation and stability. Thrombospondins are released from astrocytes and promote synaptogenesis (Christopherson *et al.*, 2005). These molecules induce the structural formation of new synapses that are functionally immature and cannot produce an action potential (Christopherson *et al.*, 2005). Another astrocyte signaling factor, Hevin, induces excitatory synapse formation while its inhibitor secreted protein, acidic, cysteine-rich (SPARC) prevents synapse formation (Kucukdereli *et al.*, 2011). SPARC prevents excessive excitation of synapses by controlling the level of alpha-amino-3-hydroxy-5-methyl-4-isoxazole propionic acid receptors (AMPA receptors) at the synapse (Jones *et al.*, 2011). Loss of SPARC in mice results in accumulated AMPAR at synapses and impaired synaptic plasticity (Jones *et al.*, 2011). SPARC inhibits integrin complexes associated with AMPARs (Jones *et al.*, 2011). Therefore in the absence of SPARC, sustained stability of the AMPAR at synapses is achieved resulting in increased excitatory synapse function and reduced synaptic plasticity (Jones *et al.*, 2011). Astrocyte-derived cholesterol is also required during synaptogenesis as retinal ganglion cells (RGCs) were unable to form immature synapses without cholesterol supplied by astrocytes (Mauch *et al.*, 2001). The RGCs were able to produce enough cholesterol to differentiate and extend dendrites and axons but

large amounts of cholesterol were required to form functional synapses (Mauch *et al.*, 2001).

After formation of synapses there are signals that lead to synaptic maturation and reinforce synaptic strength. Allen *et al.* identified astrocyte-secreted glypicans 4 and 6 as molecules that are able to induce functionally mature synapses (Allen *et al.*, 2012). Glypicans increase the surface level and clustering of a subunit of the AMPAR (Allen *et al.*, 2012). The authors also demonstrated that glypican 4-deficient mice had defective synapse formation and reduced amplitude of excitatory synaptic currents in the hippocampus (Allen *et al.*, 2012). Extracellular matrix components have also been implicated in reinforcing synaptic strength by stabilizing the AMPAR at synapses and preventing mobility (Frischknecht *et al.*, 2009). In another study, hippocampal neurons were cultured on an astrocyte feeder layer resulting in the formation of many synapses (Pyka *et al.*, 2011). However, with the addition of enzymes that digest certain astrocyte-secreted extracellular matrix factors these synapses became weaker and also resulted in an accumulation of immature synapses (Pyka *et al.*, 2011).

Astrocytes are important for synapse development and plasticity of neurons, but what is their role at a functional synapse? As mentioned previously, astrocytes possess glutamate transporters required for proper glutamate clearance at the synapse to prevent excitotoxicity and neurodegeneration (Rossi, 2015; Rothstein *et al.*, 1996; Sofroniew and Vinters, 2010). Astrocytes also release various “gliotransmitters”, in response to synaptic activity (reviewed in (Araque *et al.*, 2014). There are in fact many gliotransmitters that are released in response to

Ca²⁺ elevation in astrocytes, including astrocytic glutamate, ATP, D-serine, and TNF α (Araque *et al.*, 2014). Astrocytic glutamate has been implicated in modulating the frequency of excitatory and inhibitory postsynaptic potentials and of basal synaptic transmission in the hippocampus. It is also able to modulate long term depression in the cortex (Araque *et al.*, 2014). ATP has been implicated in modulation of long term potentiation, basal synaptic depression, and depression of evoked excitatory postsynaptic potentials in the hippocampus and regulation of basal synaptic transmission in the cortex (Araque *et al.*, 2014). D-serine has been strongly implicated in long term potentiation in the hippocampus and both long term potentiation and depression in the cortex. Finally TNF α has been associated with insertion of AMPARs to strengthen synapses (Araque *et al.*, 2014). Although these gliotransmitters have been implicated in neuromodulation, many mechanistic questions remain unanswered such as how certain astrocyte receptors are differentially activated to cause Ca²⁺ elevation and how this leads to the release of different gliotransmitters (Araque *et al.*, 2014). The mechanism behind the release of each gliotransmitter requires more attention to fully understand how astrocytes function at the synapse.

The plasticity of astrocyte morphology has been implicated in promoting excitatory synapse stability (Bernardinelli *et al.*, 2014). In response to synaptic activity, specifically activation of metabotropic glutamate receptors (mGluRs) by neuronal glutamate resulting intracellular Ca²⁺ signaling, PAs undergo structural remodeling to enhance active synapse coverage and synapse stability (Bernardinelli *et al.*, 2014). The authors explored this further by activating single-

synapses through photoactivation to demonstrate that this PAP mobility is synapse specific and therefore astrocytes contacting many synapses can respond to each individually (Bernardinelli *et al.*, 2014). This mobility of PAPs and their ability to respond to and strengthen individual synapses implies that astrocytes may be involved in long term potentiation and ultimately learning and memory (Bernardinelli *et al.*, 2014).

1.1.4 Astrocyte involvement in the pathology of neurodevelopmental disorders

Neurodevelopmental disorders are characterized through a set of similar symptoms such as cognitive impairments, autistic features, epilepsy and motor abnormalities. The research conducted on these disorders has focused mostly on neuronal dysfunction; however, recent studies have emerged describing a role for astrocytes as a contributor to pathology of these disorders. Autism spectrum disorder is a set of neurodevelopmental disorders without an identified single etiology, because it is most likely caused by both genetic and environmental factors (Fakhoury, 2015). Autistic patients exhibit reduced language and social skills, repetitive behaviours and with some secondary symptoms such as aggression and anxiety (Fakhoury, 2015). Postmortem brain samples from autistic patients revealed astrogliosis as indicated by elevated GFAP protein levels (Laurence and Fatemi, 2005). The mRNA levels of two astrocyte-specific glutamate transporters were also increased in patient samples, mainly from the cerebellum (Purcell *et al.*, 2001). In another study protein levels of water channel gene aquaporin 4 (Aqp4) were decreased in the cerebellum and gap junction

protein Gja1 was increased in the superior frontal cortex of autistic patients (Fatemi *et al.*, 2008). Gain-of-function mutations in another key astroglial gene, potassium channel *Kir4.1*, have been found in autistic patients with seizures indicating a possible causative mechanism for altered neuronal excitability (Sicca *et al.*, 2011). These findings indicate a pathological role for astrocytes in patients with autism. Many other neurodevelopmental disorders contain both autistic features and epilepsy, including Fragile X syndrome.

Fragile X syndrome is caused by the transcriptional silencing of fragile X mental retardation protein (FMRP), a translational repressor, due to hypermethylation of a large repeat present in the *FMR1* gene locus on the X chromosome (Verkerk *et al.*, 1991). Fragile X syndrome is the most common form of inherited intellectual disability and affected males display intellectual disability, seizures, motor abnormalities and autistic features, such as the inability to communicate effectively (Gallagher and Hallahan, 2012; Kidd *et al.*, 2014). Astrocytes lacking FMRP were co-cultured with wildtype neurons to determine if proper neuronal growth could be supported by *fmr1^{-/-}* astrocytes (Jacobs and Doering, 2010). These neurons displayed abnormal dendrite morphology and decreased levels of presynaptic and postsynaptic protein aggregates (Jacobs and Doering, 2010). This phenotype was absent when neurons were cultured with normal astrocytes, indicating *fmr1^{-/-}* astrocytes cannot support proper neuronal growth and synapse formation (Jacobs and Doering, 2010). Another study determined that astroglial glutamate transporter Slc1a2 protein levels were reduced in the *fmr1^{-/-}* mouse cortex and this resulted in reduced glutamate uptake (Higashimori *et al.*, 2013). The authors determined that

fmr1^{-/-} astrocytes expressed similar levels of Slc1a2 when compared to wildtype astrocytes but could not upregulate Slc1a2 expression in response to neurons (Higashimori et al., 2013). This was a result of loss of mGluR5 receptor, which was regulated by FMRP (Higashimori et al., 2013). The above evidence therefore indicates astrocytes as important contributors to Fragile X syndrome pathologies.

Rett syndrome is caused by loss of function mutations in an X-linked gene called *MeCP2* (Amir et al., 1999). The methyl CpG binding protein 2 (MeCP2) protein is a chromosomal protein that preferentially binds 5-methyl cytosine in CpG dinucleotides (Lewis et al., 1992). This protein functions as a transcriptional repressor by changing chromatin structure, making genes more or less accessible (Nan et al., 1998). Baby girls affected by this disorder initially appear normal but exhibit developmental and cognitive regression at 12 to 18 months of age along with loss of verbal skill and motor abnormalities (Dolce et al., 2013). Recent literature describes a cell non-autonomous role for astrocytes in Rett syndrome pathology. Ballas et al. found that MeCP2 was lost in both neurons and astrocytes in Rett syndrome brains (Ballas et al., 2009). They also determined that wildtype neurons cultured with mutant astrocytes from a Rett syndrome mouse model, or treated with mutant astrocyte-derived media, resulted in abnormal dendrite morphology (Ballas et al., 2009). Astrocytes lacking MeCP2 grew significantly slower than wildtype astrocytes and MeCP2 levels in heterozygous female (*MeCP2*^{+/-}) cultured astrocytes decreased when left in culture for longer than 2 weeks (Maezawa et al., 2009). *MeCP2* transcript levels remained the same in these cells and inhibition of astrocyte gap junctions prevented the spread of

MeCP2 deficiency through astrocytes (Maezawa *et al.*, 2009). MeCP2-null astrocytes have altered expression of several astroglial genes and impaired glutamate clearance *in vitro* (Okabe *et al.*, 2012). An exciting rescue study re-expressed MeCP2 only in astrocytes in MeCP2-deficient mice and several symptoms were rescued, such as restored respiratory abnormalities, improved locomotion and prolonged life span (Lioy *et al.*, 2011). The discovery that astrocytes are defective in the brains of Rett syndrome girls confirms that astrocyte biology must be investigated to fully understand the underlying causes of neurodevelopmental disorders.

1.1.5 Alpha thalassemia mental retardation X-linked syndrome

Alpha thalassemia mental retardation, X-linked syndrome is caused by mutations in the X-linked *ATRX* gene (Gibbons *et al.*, 1995), which encodes a chromatin-remodeling protein. This syndrome affects males due to its X-linked nature and has the following symptoms: moderate to severe intellectual disability, characteristic facial abnormalities, alpha thalassemia blood disorder, skeletal abnormalities, microcephaly, seizures, genital abnormalities (Gibbons, 2006) and myelination defects (Wada *et al.*, 2013). ATR-X syndrome has many overlapping

Table 1. Overlapping symptoms of three neurodevelopmental disorders

Feature of disorder	Fragile X Syndrome	Rett Syndrome	ATR-X syndrome
Cognitive Impairment	✓	✓	✓
Autistic features	✓	✓	✓
Epilepsy	✓	✓	✓
Motor abnormalities	✓	✓	✓
Abnormal expression of a chromatin remodeling protein	X	✓	✓

features with Rett Syndrome and Fragile X syndrome (Table 1). Furthermore MeCP2 interacts with ATRX, and this interaction is important for ATRX recruitment to sites of heterochromatin (Nan *et al.*, 2007). These observations suggest an overlap at both the phenotypic and molecular level between these neurodevelopmental disorders.

1.2 ATRX is a key regulator of chromatin structure

1.2.1 Gene location and protein structure

The *ATRX* gene is located on the X chromosome at Xq13.3 (Gibbons *et al.*, 1995) and undergoes X inactivation (Gibbons *et al.*, 1992). This gene contains 36 exons and is 300 kb long, giving rise to a 280 kDa protein (Picketts *et al.*, 1996) that is ubiquitously expressed in humans and mice (Gecz *et al.*, 1994; Stayton *et al.*, 1994). A 200 kDa truncated form of ATRX, ATRXt, was reported (Berube *et al.*, 2000; McDowell *et al.*, 1999) and shown to result from alternative splicing of the gene (Garrick *et al.*, 2004). ATRX has two highly conserved domains (Picketts *et al.*, 1998): the N-terminal ATRX-DNMT3-DNMT3L (ADD) domain that is homologous to the DNA methyltransferase family (Aapola *et al.*, 2000) and the C-terminal Swi/Snf helicase domain that contains an ATPase/helicase motif (Picketts *et al.*, 1996) (Figure 3).

The ADD domain recognizes modified histone tails, specifically H3K9me3 in combination with unmethylated H3K4 (Dhayalan *et al.*, 2011; Eustermann *et al.*, 2011; Iwase *et al.*, 2011). The switch/sucrose-nonfermenting (SWI/SNF) domain

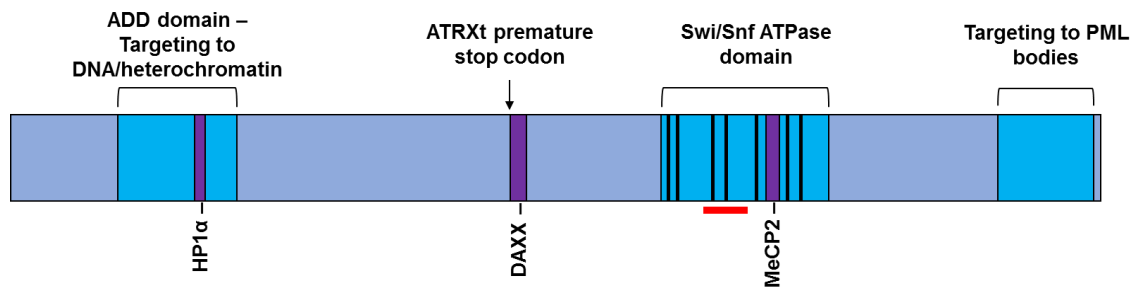


Figure 3. Schematic of ATRX protein. The conserved domains ADD, Swi/Snf and PML body (promyelocytic leukemia body) targeting domains are indicated by the blue regions while protein interaction sites are indicated by purple regions. The ATRXt premature stop codon that gives rise to the truncated form of ATRX is represented by the arrow. The seven highly conserved collinear helicase domains in the Swi/Snf domain are represented by the vertical black lines in the conserved domain region. The red line indicates the approximate location of the *loxP* sites inserted in the *Atrx* floxed mice used in this work. Figure adapted from review by Nathalie Bérubé (Berube, 2011).

closely resembles the Rad54 family of proteins (Picketts *et al.*, 1998) and is characterized by seven highly conserved collinear helicase domains (Picketts *et al.*, 1998) that confer the ATPase and chromatin-remodeling activities of ATRX (Tang *et al.*, 2004). ATRX associates with many proteins such as heterochromatin-associated protein 1 alpha (HP1 α) (Berube *et al.*, 2000; McDowell *et al.*, 1999), death-associated protein 6 (Daxx) (Tang *et al.*, 2004; Xue *et al.*, 2003), and methyl-CpG-binding protein (MeCP2) (Nan *et al.*, 2007) (Figure 3). A proportion of ATRX and Daxx colocalize to promyelocytic leukemia nuclear bodies (PML bodies) in the nucleus (Xue *et al.*, 2003). The conserved domains of the ATRX protein and the aforementioned protein-protein interactions are vital for its diverse cellular functions. The majority of disease-causing mutations map within the ADD and SWI/SNF domains of ATRX and result in reduced expression or activity of the protein (Gibbons *et al.*, 1995; Picketts *et al.*, 1996).

1.2.2 ATRX's diverse functions in the cell and at chromatin

ATRX is an exclusively nuclear protein and associates with pericentromeric heterochromatin throughout all stages of the cell cycle (Berube *et al.*, 2000; McDowell *et al.*, 1999). ATRX also associates with highly repetitive sequences in both telomeres and euchromatin (Law *et al.*, 2010). ATRX interacts with heterochromatin through its N-terminal domain (McDowell *et al.*, 1999), particularly using its ADD domain to bind H3K9me3 (Dhayalan *et al.*, 2011). ATRX is also phosphorylated in a cell cycle dependent manner (Berube *et al.*, 2000).

ATRX and its binding partner Daxx localize to pericentric heterochromatin DNA repeats and telomeres and control transcription of these repeats by integrating histone variant H3.3 into nucleosomes (Drane *et al.*, 2010; Goldberg *et al.*, 2010). H3.3 is a replication independent histone variant that is associated with open and active chromatin (Loyola *et al.*, 2006). ATRX binds Daxx/H3.3 to target repetitive sequences to deposit H3.3 (Drane *et al.*, 2010). Loss of ATRX in the neonatal forebrain resulted in altered transcript levels of a subset of genes, including ancestral pseudoautosomal genes and a network of imprinted genes (Kernohan *et al.*, 2010; Levy *et al.*, 2008). The method of imprinted gene regulation was further investigated, leading to the model in which ATRX and MeCP2 position nucleosomes around CCCTC-binding factor (CTCF) binding sites (Kernohan *et al.*, 2014). CTCF is involved in chromatin looping to separate or bring together enhancers and/or repressor and regulate the expression of nearby genes (Ong and Corces, 2014). Through regulation of chromatin looping, ATRX and MeCP2 can coordinate gene expression of selected imprinted genes (Kernohan *et al.*, 2014). Another mechanism for ATRX regulation of gene expression in a subset of genes, including autism susceptibility gene Neuroligin 4, is the incorporation of H3.3 at G-rich regions of the gene body (Levy *et al.*, 2015). ATRX was found to interact with G-quadruplexes, a secondary structure that forms in regions of DNA rich in guanine, *in vitro* (Law *et al.*, 2010) and ATRX-null neuroprogenitors treated with a drug that stabilizes G-quadruplex formation had increased DNA damage (Watson *et al.*, 2013). Levy *et al.* determined that ATRX deficiency in the mouse forebrain resulted in decreased H3.3 incorporation and stalled RNA polymerase II

at G-rich intragenic sites (Levy *et al.*, 2015). These findings suggest that ATRX helps resolve G-quadruplex formation through H3.3 deposition at these regions to allow transcriptional elongation (Levy *et al.*, 2015).

Loss of ATRX also results in replication and mitotic abnormalities. ATRX depletion in human HeLa cells led to many mitotic defects including: prolonged prometaphase to metaphase transition, abnormal sister chromatid congression and reduced sister chromatid cohesion at the metaphase plate, chromosome decondensation and overall lengthening of mitosis (Ritchie *et al.*, 2008). Micronuclei, pyknotic nuclei and misaligned chromosomes were also identified *in vivo* in embryonic mouse brain sections (Ritchie *et al.*, 2008). Interestingly, ATRX depletion in mouse myoblasts also led to mitotic defects, genomic instability, telomere defects and p53 accumulation (Huh *et al.*, 2012). *Atrx* deletion resulted in increased sensitivity to replication stress-inducing agents with increased double strand breaks, increased S phase population, and accumulated DNA damage at telomeres (Leung *et al.*, 2013; Watson *et al.*, 2013). Proper replication restart after DNA damage, prevention of replication fork stalling and progression through S-phase also require ATRX (Clynes *et al.*, 2014; Leung *et al.*, 2013). ATRX is important for proper meiotic spindle organization and chromosome alignment in meiosis in the mouse oocyte (De La Fuente *et al.*, 2004).

1.2.3 ATRX and neuronal development

ATRX is important in neurons during development, as exhibited by mouse models with both loss and overexpression of ATRX. One model using transgenic mice that

overexpress ATRX exhibited embryonic lethality and those pups that did survive exhibited craniofacial abnormalities and disorganization of the proliferative neuroepithelium (Berube *et al.*, 2002). Berube *et al.* created a mouse model that used Cre recombinase mediated deletion of *Atrx* by flanking exon 18 with *loxP* sites under the control of the *Foxg1* promoter (Berube *et al.*, 2005). *Foxg1* expression is confined to the forebrain in mice and expression begins at E8.5, causing conditional deletion of ATRX in these cells (Hebert and McConnell, 2000). Male mice lacking ATRX in the forebrain were smaller in length and weight than their wildtype counterparts and exhibited cortical and hippocampal size reduction (Berube *et al.*, 2005). These regions were hypocellular due to increased apoptosis and not a defect in proliferation (Berube *et al.*, 2005). This cell death in the ATRX-null forebrain was determined to be p53-mediated as deletion of both ATRX and p53 rescued cell death in the brain (Seah *et al.*, 2008).

Further investigation of these mice with conditional inactivation of ATRX specifically in the embryonic forebrain revealed increased DNA damage through γ H2AX (a marker for double-stranded breaks) immunostaining, and these cells also had elevated levels of cleaved caspase 3, an apoptosis marker (Watson *et al.*, 2013). These mice also exhibited systemic effects, such as reduced life span, heart enlargement, decreased bone mineral density and reduced circulating levels of thyroxine and IGF-1, due to ATRX being deleted in the anterior pituitary as well as the forebrain (Watson *et al.*, 2013). Another study using the same mouse model found an increase in cell-cycle exit in early to mid-neurogenesis and a depletion in progenitor cells leading to disproportionate layering of neurons in the cortex

(Ritchie *et al.*, 2014). ATRX was also required for correct timing of neuroprogenitor differentiation (Ritchie *et al.*, 2014). These findings ascertained the importance of ATRX in neurons. However, our understanding of ATRX function in other cell types of the central nervous system, such as astrocytes, is severely lacking. As previously mentioned, MeCP2-null astrocytes display growth defects, and co-culture with wild-type neurons demonstrated that MeCP2-deficient astrocytes are unable to support dendritic growth and maturation (Ballas *et al.*, 2009; Maezawa *et al.*, 2009). Given that MeCP2 deficient astrocytes fail to recruit ATRX to chromatin, we predict that ATRX-null astrocytes will display similar defects. This question can be addressed by developing a model of ATRX inactivation specifically in astrocytes and this was the main goal of the present thesis.

1.3 Hypothesis and Summary of Findings

The role of astrocytes in the pathology of neurodevelopmental disorders is an emerging focus of research. With cell non-autonomous effects on neurons demonstrated in similar neurodevelopmental disorders, the role for astrocytes in ATR-X syndrome pathology requires investigation. I hypothesize that ATRX is important for proper astrocyte development and function and that creation of a novel mouse model will allow the study of ATRX in astrocytes.

The effect of *Atrx* deletion in astrocytes was assessed in a mouse model where ATRX is conditionally deleted in the forebrain (Berube *et al.*, 2005). The protein levels of ALDH1L1, an astrocyte-specific marker, were decreased in the cKO males but this decrease was variable between 3 control and cKO pairs and did not

reach significance. Cell counts were performed to determine whether this decrease in ALDH1L1 is due to decreased protein expression per cell or a decrease in astrocyte population. There was a slight, but non-significant decrease in Aldh1l1 positive nuclei in the cKO. Variability in astrocyte number between control and cKO pairs was observed. Analysis of a previously performed microarray revealed altered expression of astrocyte-enriched genes and gene ontology analysis determined enriched, altered astrocyte functional pathways in cKO males when compared to controls.

Mice with inducible and conditional inactivation of *Atrx* in astrocytes were created. *Atrx* deletion in astrocytes was validated through hippocampal cell counts revealing GFAP positive cells lacking ATRX at P26. Immunofluorescence staining for ATRX, DAPI and GFAP in the cerebellum revealed many nuclei lacking ATRX staining. Measurement of *Atrx* mRNA levels in the hippocampus and cortex of inducible KOs revealed no significant difference when compared to controls. To further investigate the induction of Cre recombinase by tamoxifen, a double fluorescent reporter allele was utilized. This allele expresses GFP in response to Cre recombinase activity, and therefore in astrocytes in response to tamoxifen treatment in this model. GFP expression in the cortex and hippocampus was only present in males carrying the inducible Cre recombinase allele in response to tamoxifen.

Assessment of astrocyte domain size and morphology was accomplished through use of the previously mentioned double fluorescent reporter allele. The inducible KO demonstrated larger astrocyte domains and an increased amount of GFP

domain induction by tamoxifen. This indicated that more astrocytes are responding to tamoxifen-mediated recombination. The larger domains observed may be due to larger astrocyte domains or to increased overlap between separate astrocyte domains. qRT-PCR of astroglial genes demonstrated a decrease in *connexin 30*, a component of astrocyte gap junctions, expression. Although this decrease did not reach significance, additional biological replicates should be analyzed to investigate the possible altered levels in the inducible KO. Decreased expression of Connexin 30 could lead to communication defects between astrocytes as it is one of only two gap junction proteins connecting the astroglial network.

2 Materials and Methods

2.1 Animal Husbandry and Genotyping

Several mouse lines were used throughout the following studies and these are summarized in Table 2. *Atrx^{loxP}* (or *Atrx^{fl/fl}*) mice containing *loxP* sites flanking intron 18 of *Atrx* (Figure 4) were kindly provided by D. Higgs (Weatherall Institute of Molecular Medicine, John Radcliffe Hospital, Oxford, United Kingdom). Recombination of these *loxP* sites result in the deletion of exon 18, which is equivalent to a null mutation of *Atrx* (Figure 4) (Berube *et al.*, 2005).

First, conditional deletion of *Atrx* in the mouse forebrain was achieved by crossing *Atrx^{fl/WT}* female mice (129Sv background) with heterozygous *FoxG1-Cre recombinase* knock-in males (129Sv/FVBN background). The *FoxG1-Cre recombinase* mice were originally obtained from S. McConnell (Stanford

University, Stanford, California, USA). Cre recombinase driven by the *FoxG1* promoter directs recombination and silencing of *Atrx* in cells with the *loxP* allele in the mouse forebrain beginning at embryonic day 8.5 (E8.5, (Hebert and McConnell, 2000)). Male offspring of this cross resulted in two genotypes used in this study: *Atrx^{f/Y}FoxG1-Cre⁺*, who lack ATRX in the forebrain, and *Atrx^{WT/Y}FoxG1-Cre⁺*, who will still express ATRX despite also expressing Cre recombinase but lack the *loxP*-flanked *Atrx* allele.

Secondly, to achieve spatial and temporal deletion of *Atrx* in astrocytes, *Atrx^{f/WT}* female mice were crossed to males carrying the transgenic *Glast-Cre^{ERT}* recombinase allele (Mori *et al.*, 2006; Slezak *et al.*, 2007) (Jackson Laboratory, C57BL/6 background). *Glast-Cre^{ERT}* allele expresses Cre recombinase in response to tamoxifen treatment in retinal muller glia, Bergmann glia in the cerebellum, astrocytes, and neural progenitors in the dentate gyrus (Mori *et al.*, 2006; Slezak *et al.*, 2007). The Cre recombinase enzyme is fused to the estrogen receptor and stimulation with tamoxifen leads to translocation of the enzyme into the nucleus where it can induce recombination. *Atrx^{f/Y}Glast-Cre^{ERT}* mice will delete *Atrx* in response to tamoxifen while the control males, *Atrx^{WT/Y}Glast-Cre^{ERT}*, will have active Cre recombinase with the addition of tamoxifen but will still express the wildtype *Atrx* allele.

Finally, females heterozygous for the *Atrx* floxed allele and carrying a knock-in double reporter allele, *mT/mG^{WT/+}* (129Sv background), were also crossed with *Glast-Cre^{ERT}* males. This double reporter allele, driven by the chicken β -actin promoter, causes ubiquitous expression of tdTomato (*mT*) (Muzumdar *et al.*,

2007). The coding sequence of membrane-targeted tdTomato is flanked by *loxP* sites (Muzumdar *et al.*, 2007). Upon Cre-activation, the tdTomato sequence is excised and membrane-targeted enhanced green fluorescent protein (GFP) is then expressed (mG) (Muzumdar *et al.*, 2007) (Figure 5). This means that cells expressing Cre-recombinase driven by the *Glast* promoter will switch from tdTomato fluorescence to GFP fluorescence upon tamoxifen administration. *Atrx^{f/y}Glast-Cre^{ERT}mT/mG^{WT/+}* astrocytes will lack ATRX and exhibit GFP fluorescence in response to tamoxifen administration. *Atrx^{WT/y}Glast-Cre^{ERT}mT/mG^{WT/+}* astrocytes will still express ATRX but will also express GFP due to the activation of Cre recombinase by tamoxifen. Mice lacking the *Glast-Cre^{ERT}* allele but carrying the *mT/mG* allele will only express tdTomato fluorescence.

For genotyping, tail or ear notch samples from mice were digested and genomic DNA was extracted using DirectPCR and proteinase K (Thermo Scientific). DNA from these samples was then genotyped by PCR using primer sets for *Atrx* (17F, 18R and *neoR*), *Glast-Cre^{ERT}* (GlastF, GlastR), *mT/mG* (*mT/mG⁺* F, *mT/mG⁺* R), and *Sry* (SryF and SryR), as listed in Table 3. Placement of *loxP* sites in the *Atrx* gene is indicated by Figure 4, which also corresponds to primers used to genotype the *Atrx* gene in Table 3.

2.2 Tamoxifen Preparation and Injection

Tamoxifen (≥99%, Sigma) was diluted to 10 mg/mL for tamoxifen injections. The appropriate amount of the drug was measured and dissolved in ethanol (95%) at

Table 2. Summary of mouse genotypes used within this thesis, grouping control and knockout pairs compared by colour.

Genotype	Description	Referred to as
<i>Atrx</i> ^{WT/Y} <i>FoxG1-Cre</i> ⁺	<i>Cre recombinase</i> positive control	Control
<i>Atrx</i> ^{f/Y} <i>FoxG1-Cre</i> ⁺ ,	Conditional inactivation in forebrain cells	cKO
<i>Atrx</i> ^{WT/Y} <i>Glast-Cre</i> ^{ERT}	Inducible <i>Cre recombinase</i> positive control	Control
<i>Atrx</i> ^{f/Y} <i>Glast-Cre</i> ^{ERT}	Inducible inactivation in astrocytes	Inducible KO
<i>Atrx</i> ^{WT/Y} <i>Glast-Cre</i> ^{ERT} <i>mT/mG</i> ^{WT/+}	Fluorescent <i>Cre recombinase</i> positive control	Fluorescent Control
<i>Atrx</i> ^{WT/Y} <i>Glast-Cre</i> ^{ERT} <i>mT/mG</i> ^{WT/+}	Fluorescent inducible knockout in astrocytes	Fluorescent Inducible KO

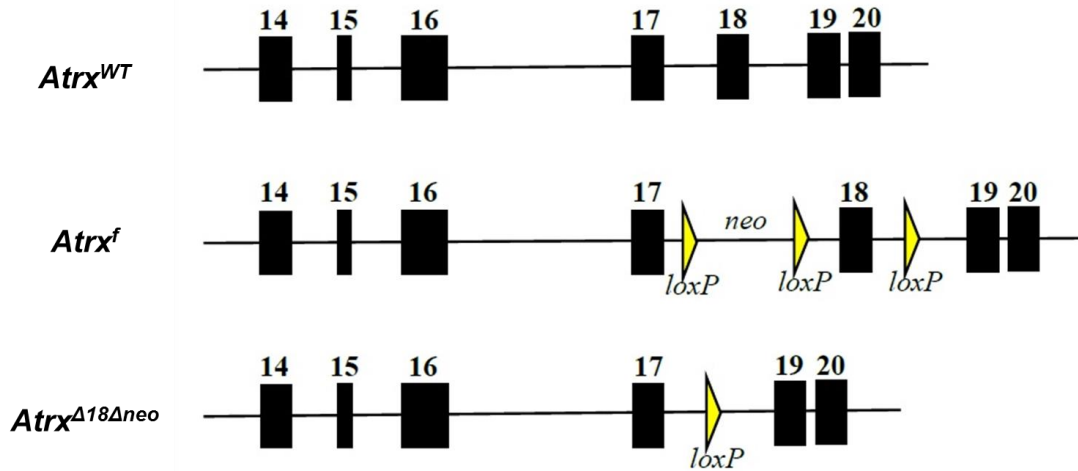


Figure 4. *LoxP* site placement in *Atrx* gene. Blocks and corresponding numbers represent respective exons in the *Atrx* gene. The top line indicates the wildtype *Atrx* allele (*Atrx*^{WT}). The middle line shows the insertion of *loxP* sequences flanking exon 18 along with a *neo* marker (*Atrx*^f). The bottom line demonstrates the recombination of *Atrx* upon *Cre recombinase* activation in which exon 18 and the *neo* cassette have been removed (*Atrx*^{Δ18Δneo}).

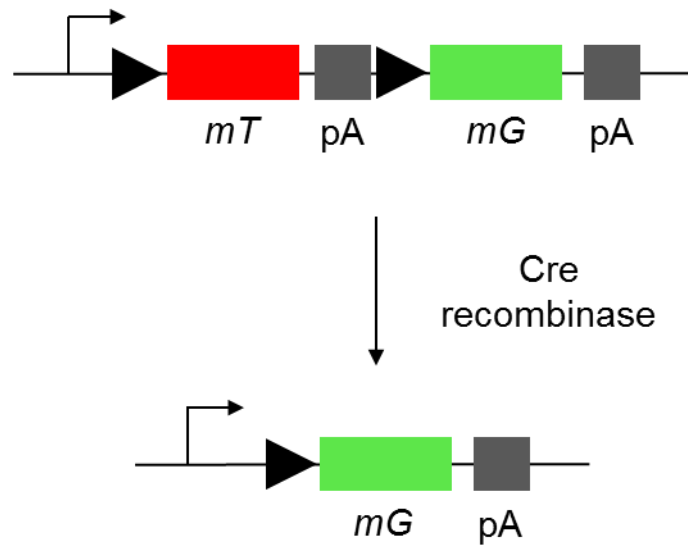


Figure 5. Schematic representation of the *mT/mG* fluorescent reporter allele.

The *mT/mG* allele under the control of the chicken β -actin promoter with flanking *loxP* sites around the tdTomato allele (*mT*) (represented by arrows). After Cre recombinase is activated, the tdTomato sequence is excised allowing expression of membrane-targeted enhanced green fluorescent protein (GFP or *mG*). The arrow indicates direction of transcription and pA denotes polyadenylation sites present. Adapted from Muzumdar *et al.* (2007).

Table 3. List of Primers used for genotyping

Primer Name	Sequence (5' to 3')
<i>Atrx</i> 17F	AGAACCGTTAGTGCAGGTTCA
<i>Atrx</i> 18R	TGAACCTGGGGACTTCTTTG
<i>Atrx neo^R</i>	CCACCATGATATTCGGCAAG
<i>Sry</i> F	GCAGGTGGAAAAGCCTTACA
<i>Sry</i> R	AAGCTTTGCTGGTTTTTGGGA
<i>Glast</i> F	ACAATCTGGCCTGCTACCAAAGC
<i>Glast</i> R	CCAGTGAAACAGCATTGGTGTC
<i>mT/mG⁺</i> F	CTCTGCTGCCTCCTGGCTTCT
<i>mT/mG⁺</i> R	TCA ATG GGCGGGGGTCGTT

10% of the final volume. This solution was heated at 65°C until the tamoxifen was completely dissolved. Ninety percent of the total volume of corn oil (Sigma) was added to the ethanol-tamoxifen solution to achieve the desired concentration of 10 mg/mL.

Two injection protocols were used in this study. Adult males (3 months) were injected intraperitoneally with 2 mg of tamoxifen (200 μ L of 10 mg/mL) daily for 5 days. These control and inducible knockout males were then sacrificed 1 week post-final injection for experimental analysis. Males were also injected at an earlier time point. Intraperitoneal injections of 1 mg of tamoxifen (100 μ L of 10 mg/mL) began at postnatal day 10 (P10) and continued daily for 3 days until P12. Control and inducible knockout males were then sacrificed 2 weeks post-final injection at P26.

2.3 Western Blot Analysis

Tissue was mixed with cold RIPA buffer (50 mM Tris, pH 8.0, 150 mM NaCl, 1% NP-40, 0.5% deoxycholic acid, 0.1% SDS, 0.2 mM PMSF, 0.5 mM NaF, 0.1 mM Na_3VO_4) (3 mL per gram of tissue) and homogenized and incubated on ice for 30 minutes. The samples were then centrifuged at 4°C at 15800 g for 30 minutes and the supernatant transferred to a new, cold 1.5 mL Eppendorf tube, discarding the cell pellet. The protein concentration was then measured using a Bradford assay

(BioRad). Protein extracts were stored at -80°C . The samples were thawed when required and denatured at 90°C for 10 minutes.

Polyacrylamide gels, including a separating gel (10%) and a stacking gel (4%) were generated and 25 μL of each sample in 1x loading buffer were loaded into the gel along with 8 μL of protein ladder (BioRad). Gels were run at 90V for 30 minutes, then 125-130 V for 2 hours in 1x running buffer. Once adequate protein separation was achieved, the gels were transferred to nitrocellulose membranes (BioTraceTM, Pall Life Sciences) and run at 75 V for 2 hours in 1x transfer buffer. The transferred nitrocellulose membranes were blocked for 1 hour with 5%-milk-TBST. Primary antibody diluted in 5%-milk-TBST was added and the membrane was incubated at 4°C overnight. Membranes were then washed with 1x TBST and secondary antibody diluted in 5%-milk-TBST was added. The membrane was incubated in the secondary antibody for 1 hour and then washed with 1x TBST. ECL (enhanced chemiluminescence) solution was then added to membrane for approximately one minute. The membranes were then imaged using the BioRad ChemiDoc MP imaging system. Antibodies and respective dilutions are displayed in Table 5. An unpaired t-test was performed to reveal significance between control and cKO mice ($p < 0.05$).

2.4 Quantitative Real Time PCR (qRT-PCR)

The brain samples were extracted at various timepoints (P26 or 3 months) depending on the experiment. The cortex and hippocampus were isolated and stored at -80°C . RNA was then extracted from thawed samples using the RNeasy[®]

Mini or Micro Kit (Qiagen). The extracted RNA was then reverse transcribed into cDNA by the following protocol: RNA (1 µg), DEPC-H₂O and random primers were heated for 10 minutes at 65°C, and then incubated on ice for two minutes. Next, 5X first strand buffer, 100 mM DTT, 25 nM dNTPs, Superscript Reverse Transcriptase, RNA guard and more DEPC-H₂O were added to the reaction mixture. Control reactions lacking reverse transcriptase were performed to ensure reagents were not contaminated. The reaction mixture was then incubated first for 10 minutes at 30°C and then for 45 minutes at 42°C. The resulting cDNA was quantified and stored at -20°C.

qRT-PCR was performed on the cDNA prepared from extracted RNA. Primers used are listed in Table 4. cDNA was mixed with primers, H₂O and iQTM SYBR[®] Green mastermix (BioRad) and run through the following conditions on a Chromo-4 thermocycler to amplify transcripts of interest: 30-35 cycles of 95°C for 10 seconds, 55°C for 20 seconds and 72°C for 30 seconds. A final melting curve was generated in increments of 1°C per plate read. Gene expression analysis was performed using Opticon Monitor 3 and GeneX (Biorad) software. Analysis of each cDNA sample was performed in duplicate for each primer set and gene expression was normalized to *Gapdh* expression levels. An unpaired t-test was performed to reveal significance between control and inducible KO mice ($p < 0.05$). 20 µL of qRT-PCR product was run on a 1.5% agarose gel by electrophoresis to ensure band size of amplified cDNA matched the transcript of interest.

2.5 Immunofluorescence and Cell Counts

Brains were dissected and perfused with 4% PFA at varying ages (P7, P20, P26, 3 months) and were embedded in OCT (optimal cutting temperature) medium and snap frozen in liquid nitrogen. The samples were then stored at -80°C until cryosectioned sagittally or coronally at a thickness of 8 μ M. Sections used for immunofluorescence were thawed at room temperature for 1 hour. Matched slides between pairs (control and knockout) were then rehydrated in 1x PBS. The slides were then placed into warm sodium citrate for antigen retrieval and microwaved on the low heat setting for 10 minutes. Slides were then cooled in sodium citrate for 20 minutes and then washed with 1x PBS once and twice with 1x PBS+0.3% TritonX-100 to permeabilize the cell membranes. Primary antibody diluted in 1x PBS+0.3% TritonX-100 +1% BSA was then added to slides. Slides were incubated overnight at 4°C. The slides were then washed with 1x PBS+0.3% TX-100 three times and incubated in secondary antibody diluted in 1x PBS+0.3% TritonX+1% BSA for 1 hour at room temperature in the dark. Slides were then washed with 1x PBS+0.3% TritonX-100 twice and counterstained with DAPI. After washing slides with 1x PBS+0.3% TritonX-100 twice and 1x PBS once, slides were mounted and imaged using one of three microscopes: Leica CTR 6500 microscope, ZEISS Axioscop40 microscope and Leica DM5500B microscope. Figure 6A is an example of a sagittal section and the areas of interest in this study. The hippocampus is imaged many times in this study and its components have been labeled in Figure 6B. A list of primary and secondary antibodies used, and their respective dilutions, in this study are represented in Table 5. Blind cell counts were performed on many

of these slides for different experiments throughout this work. Volocity software was used to set the pixel/ μm for each microscope and create a fixed area that remained the same for each image analyzed. This fixed area was placed on each image and cell counts were performed within its boundaries.

2.6 Microarray Analysis

A microarray was performed comparing *Atrx^{f/y}FoxG1-Cre⁺* (conditional knockout) and *Atrx^{WT/y}FoxG1-Cre⁻* (control) males at P17 (unpublished, Michael Levy). Three P17 control and conditional knockout male forebrains were dissected and total RNA was extracted using the RNeasy Mini kit (Qiagen). cRNA was generated and hybridized to an Affymetrix Mouse Genome 430 2.0 Array at the London Regional genomics Center (London, Canada). One microarray chip per mouse was used and probe intensities were measured using GCOS1.4 (Affymetrix Inc.). Specific genes enriched in the astrocyte population were selected from this microarray based on a recently published study that generated a transcriptome database comparing 8 cell types in brain (Zhang et al., 2014). The top 48 genes that were enriched by more than 30 fold in astrocytes were selected and the intensity of RNA binding to each genetic probe was assessed. Heat maps indicating intensity of probe binding for each sample were generated using Partek software. Gene ontology (GO) analysis was performed on genes with altered expression. Gene levels were calculated using RMA preprocessor in GeneSpring GX 7.3.1 (Agilent Technologies Inc.) and fold-change calculated using $p < 0.05$.

Table 4. Primers used for qRT-PCR.

Primer Name	Sequence (5' to 3')
<i>Atrx</i> 17F	AGAACCGTTAGTGCAGGTTCA
<i>Atrx</i> 18R	TGAACCTGGGGACTTCTTTG
<i>Gapdh</i> F	CAACGACCCCTTCATTGACCT
<i>Gapdh</i> R	ATCCACGACCGACACATTGG
<i>Gjb6</i> F	GCCCTGGAGAACAAGACTCA
<i>Gjb6</i> R	CTCATCACCCCACACTTCCT
<i>Gja1</i> F	GAGAGCCCGA ACTCTCCTTT
<i>Gja1</i> R	TGGAGTAGGCTTGGACCTTG
<i>Slc1a2</i> F	AGATCATCGCCATCAAGGAC
<i>Slc1a2</i> R	TCCAAGCAACGGAAGGTAAC

Table 5. List of antibodies used for immunofluorescence (IF) and western blot (WB) experiments

Antibody	Description and company	Dilution used in IF and WB
GFAP	Mouse monoclonal antibody, Sigma	IF: 1:100 WB: 1:2000
ATRX H-300	Rabbit polyclonal antibody, Santa Cruz	IF: 1:100
ALDH1L11	Mouse monoclonal antibody, Millipore	IF: 1:50 WB: 1:1000
Secondary antibody - red	Alexa Fluor 594 nm, goat anti-rabbit IgG, Life Technologies	IF: 1:800
Secondary antibody - green	Alexa Fluor 488 nm, goat anti-mouse IgG, Life Technologies	IF: 1:800
Secondary antibody - HRP	Rabbit anti-mouse IgG HRP, Santa Cruz	WB: 1:4000

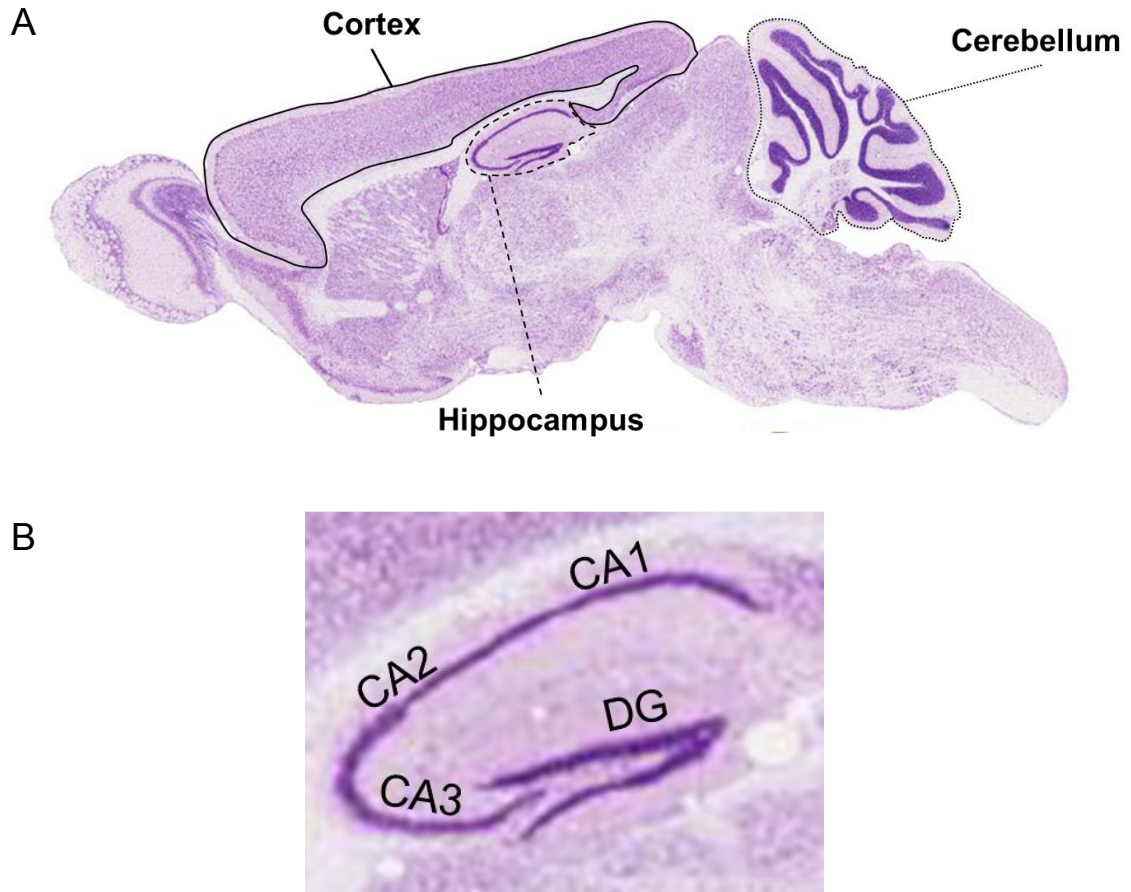


Figure 6. Regions of the mouse brain used for experimental analysis. (A) Image of a sagittal section of the mouse brain with the cortex, hippocampus and cerebellum. (B) Hippocampus enlarged and labelled for its 4 distinct regions: cornu ammonis 1 (CA1), 2 (CA2), 3 (CA3) and the dentate gyrus (DG). Images were adapted from the Allen Brain Atlas website, available online at www.brainmap.org.

3 Results

3.1 Assessing the astrocyte population in *Atrx^{f/Y}Foxg1-Cre* mice

The *FoxG1* driven Cre recombinase is active in all cell types in the forebrain and expression begins at approximately E8.5 (Hebert and McConnell, 2000). Previous studies have demonstrated that loss of ATRX in the forebrain resulted in increased DNA damage induced by replication stress and reduced cortical mass due to increased p53-mediated cell death in neuroprogenitor cells (Berube et al., 2005; Ritchie et al., 2014; Seah et al., 2008; Watson et al., 2013). What occurs in the other cell types in the *Atrx*-null forebrain has not yet been elucidated. To examine the astrocyte population, samples collected by previous graduate students (Kieran Ritchie and Matt Edwards) from previously assessed timepoints (P7 and P20, respectively) using the *FoxG1* conditional deletion of *Atrx* were analyzed. Coronal cryosections from P7 control and conditional knockouts (cKO) were stained with GFAP to determine astrocyte reactivity in an environment with neuronal cell death (Figure 7). There appears to be more reactive astrocyte activation in the cKO based on GFAP staining in outlined area (Figure 7). This result is not quantifiable and therefore a western blot assessing GFAP protein levels was performed next.

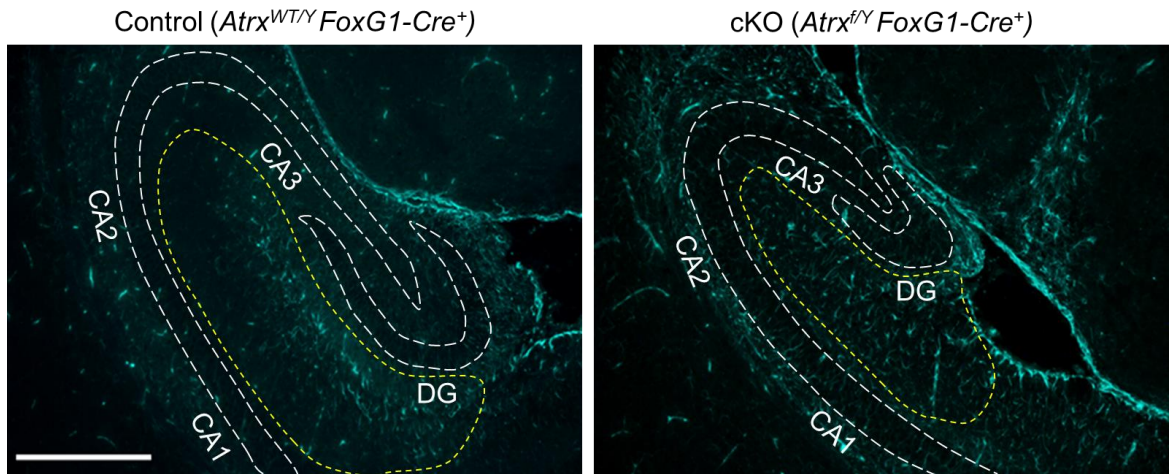


Figure 7. Potential reactive astrocyte activation in cKO hippocampus compared to control at P7. Coronal cryosections were immunostained with glial fibrillary acidic protein GFAP (green) and analysis of the hippocampus (outlined and labeled in white) revealed increased GFAP activation in the hippocampal space, outlined in yellow, in the cKO. n=2. Scale bar=205 μ m. DG=Dentate gyrus, CA1=Cornu Ammonis 1, CA2=Cornu Ammonis 2 and CA3= Cornu Ammonis 3.

To determine quantitative levels of GFAP protein levels, a Western blot was performed on P20 forebrain samples of three control and cKO pairs. ALDH1L1 levels, a cytoplasmic marker that more broadly and specifically labels astrocytes throughout the brain (Cahoy *et al.*, 2008), were also assessed. Western blot analysis of these two astrocyte markers revealed a decrease in ALDH1L1 protein levels in the cKO, however the difference was not significant (Figure 8A, B). GFAP protein levels were slightly increased, but not significantly, in the cKO compared to control (Figure 8A, B). Increased GFAP levels could indicate there are more reactive astrocytes present in the forebrain in the cKO. Decreased ALDH1L1 protein levels could indicate decreased protein levels per astrocyte or a decrease in the amount of astrocytes present in the forebrain. GFAP levels were analyzed relative to ALDH1L1 levels (Figure 8C) to determine if GFAP levels are increased per astrocyte. There is no significant difference between control and cKO GFAP/ALDH1L1 protein levels. To determine if the nonsignificant decrease in ALDH1L1 could be due to a decrease in astrocyte number, cell counts were performed.

Cell counts on P20 control and cKO coronal cryosections immunostained for ALDH1L1 and DAPI were performed where DAPI-stained nuclei surrounded by cytoplasmic ALDH1L1 staining were counted as an astrocyte. These counts were performed while blinded on three pairs of control and cKO cryosections, with 3 to 4 sections per slide. The number of astrocytes per 100,000 μm^2 for each section

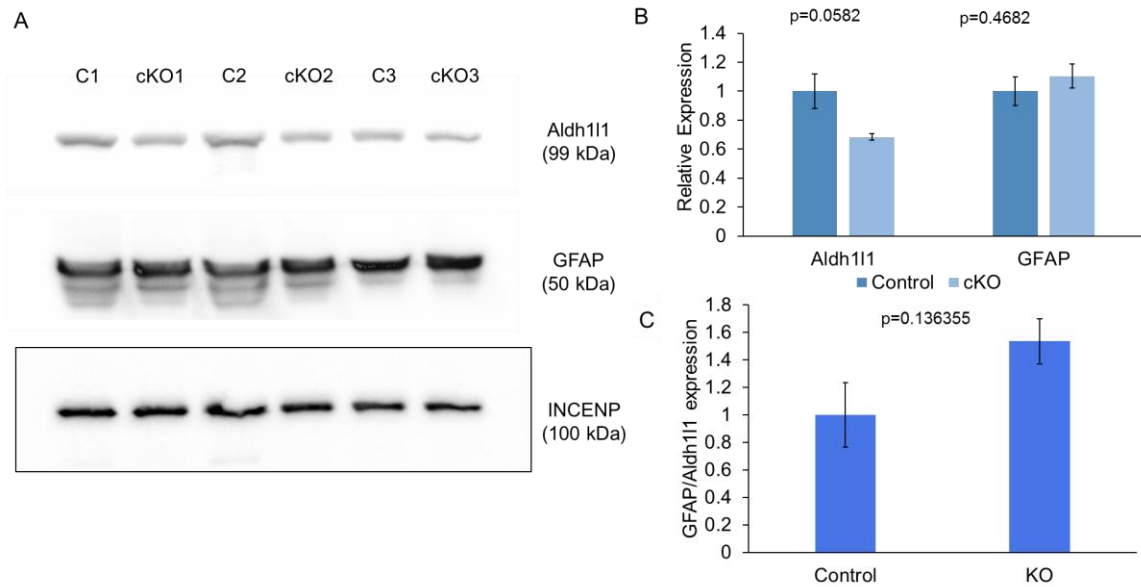
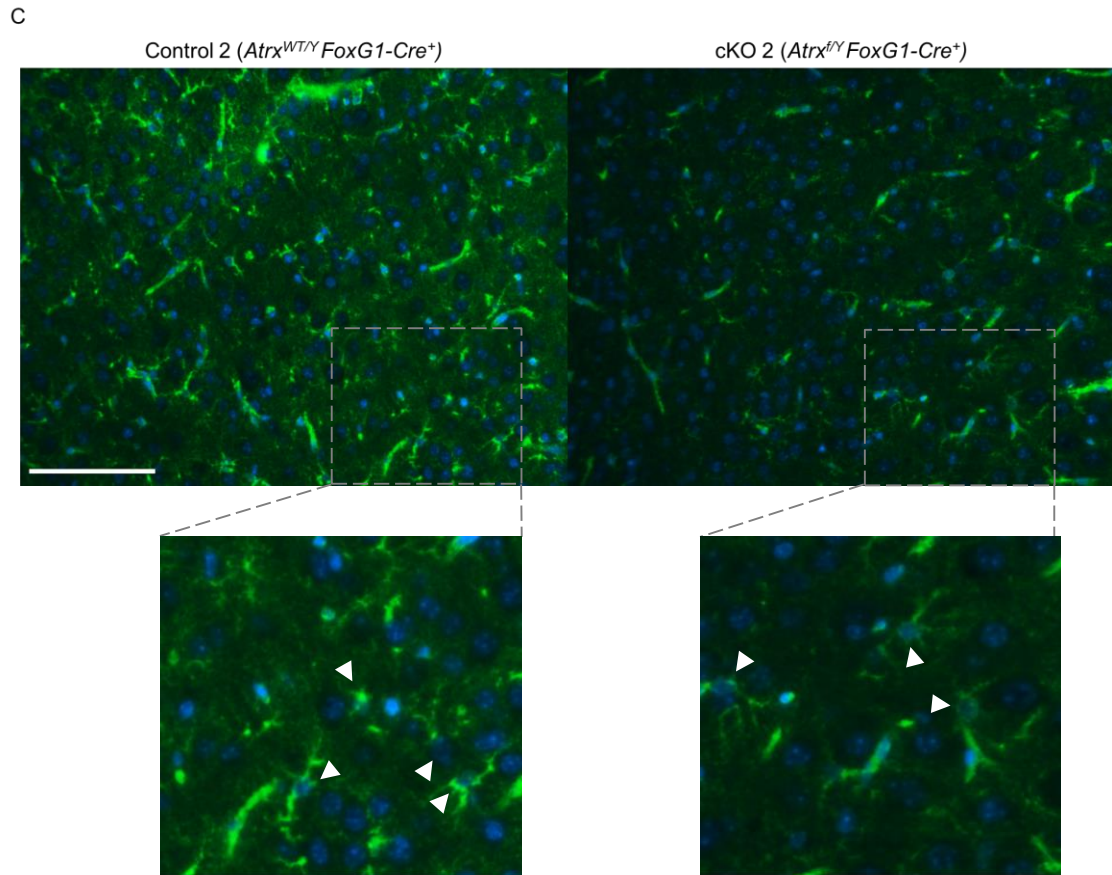
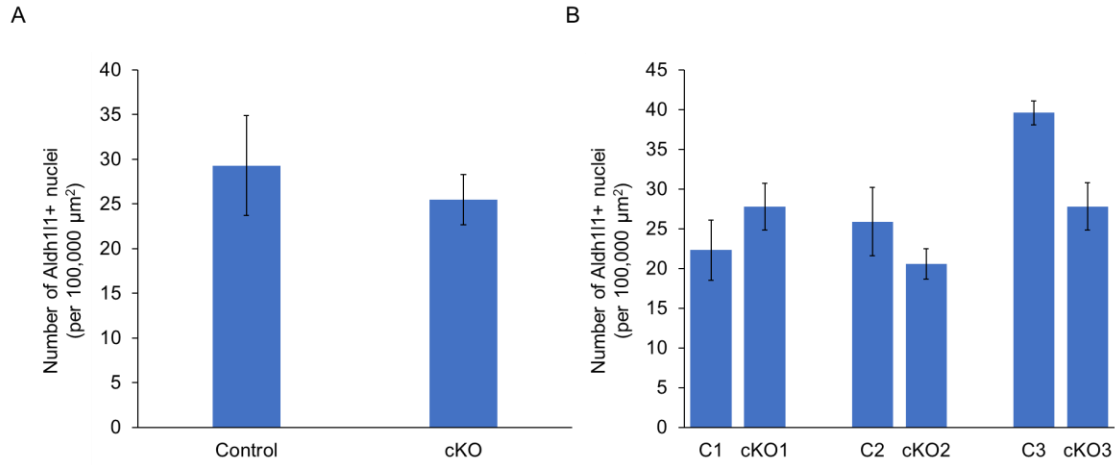


Figure 8. Quantification of ALDH1L1 and GFAP protein levels in the cKO forebrain at P20 (A) Protein extracts from control and cKO forebrain were isolated and ALDH1L1 and GFAP levels assessed via immunoblotting. (B) Quantification of protein levels revealed an insignificant decrease in ALDH1L1 in the cKO. GFAP levels remained unchanged. (C) GFAP levels were assessed relative to ALDH1L1 expression, revealing a slight but insignificant increase in the cKO. ALDH1L1 and GFAP levels normalized to INCENP levels.

was averaged for each control and cKO. The control and cKO cell counts were then averaged and this revealed no significant difference in the number of Aldh1l1 positive nuclei in cKO compared to control (Figure 9A). When assessing the individual pairs of control and cKO astrocyte cell counts, two pairs demonstrate a decrease in astrocyte number in the cKO, but one pair showed the opposite result (Figure 9B). This demonstrates a variability in the astrocyte population between pairs. Comparing immunofluorescence staining of Aldh1l1 between cKO and control mice in pair 2 revealed lower intensity of fluorescence in the cKO (Figure 9C). This is paired with a decrease in the number of astrocytes counted in pair 2 (Figure 9B). These results indicated that the amount of astrocytes in the cKO is variable between cKO males. GFAP levels may be increased relative to the number of astrocytes present in the cKO (Figure 8C), but this phenotype was also variable between cKO males (Figure 8A). Overall, we conclude that this cKO mouse model is not ideal for studying the effect of ATRX loss in astrocytes due to the non-cell-autonomous effects from ATRX deletion in other cell types, which may underlie the high variability observed between samples.

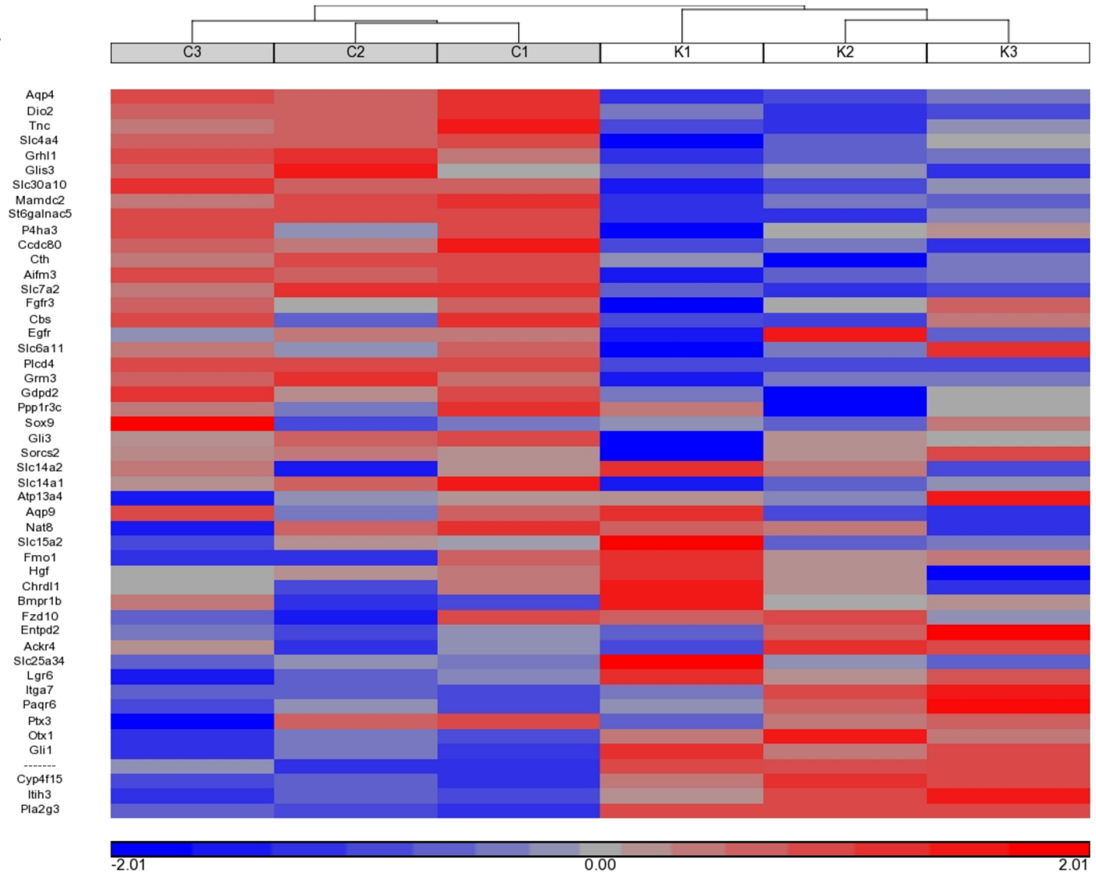
Figure 9. The number of astrocytes is not changed in the cortex of P20 cKO males compared to controls. (A) Cell counts were performed on P20 coronal cryosections of control and cKO cortex stained for ALDH1L1 and DAPI. Cell counts on 3 to 4 brain sections for each control and cKO mouse were performed and averaged per 100,000 μm^2 . (B) Cell counts of each pair of control and cKO is shown here to demonstrate variability between pairs from different litters. (C) Example of immunofluorescence staining for pair 2 (C2 and cKO2) where Aldh1l1 staining (green) surrounds DAPI stained nuclei (blue). Outlined areas of the cortex are enlarged and arrowheads indicate examples of astrocytes (ALDH1L1+ nuclei). n=3. Scale bar=100 μm .



To further examine the effects of *Atrx* inactivation in astrocytes, astrocyte-enriched genes were analyzed in a previously performed microarray comparing 3 control and 3 cKO males at P17 (unpublished, Michael Levy). To determine which genes were enriched in astrocytes a recently published RNA transcriptome comparing oligodendrocytes, neurons, microglia, astrocytes and vascular cells in the mouse cerebral cortex was used (Zhang *et al.*, 2014). The top 48 genes that were enriched more than 30-fold in astrocytes, compared to all other central nervous system cell types, were examined in the microarray (Figure 10A). Heat maps displaying the intensity of RNA-binding to each gene probe were generated, comparing 3 control and cKO males (Figure 10A). *Aqp4*, an astrocyte-specific water channel, displayed the most changed binding-intensity and is down-regulated (2-fold) in the cKO (Figure 10A). Deiodonase-2 (*Dio2*), the enzyme responsible for thyroid hormone activation was also displays lower binding intensity in the cKO and is significantly downregulated (1.6-fold), along with Tenasin C (*Tnc*) (1.6-fold), an extracellular matrix protein gene that is implicated in guidance of migrating neurons and axons during development and synaptic plasticity. *Slc4a4*, the 4th most down-regulated gene in the cKO (1.4-fold), is a protein important for glucose transport and maintaining intracellular pH. GO analysis was performed on these astrocyte-enriched genes and the top 10 altered gene groups based on biological function are shown in Figure 10B. One-carbon compound transport genes, such as those important for carbon dioxide and urea transport, were the most altered in the list of

Figure 10. Astrocyte-enriched genes demonstrate altered transcript levels in the forebrain of cKO males at P17. (A) Heat map representing the RNA-binding intensity of the top 48 astrocyte-enriched genes in a microarray performed on 3 control and 3 cKO mice. Genes listed are from most down-regulated in cKO to most upregulated, based on RNA-binding intensity. (B) Gene ontology (GO) for astrocyte-enriched genes reveals altered functional pathways in astrocytes. Heat map generation and GO analysis were performed using Partek software, $p < 0.05$, C=control, K=conditional knockout.

A



B

Function	Type	Enrichment Score	Enrichment p-value	% Genes in group that are present
One-carbon compound transport	Biological process	16.95	4.36E-08	28.57
Integral component of membrane	Cellular component	16.41	7.47E-08	0.70
Intrinsic component of membrane	Cellular component	15.65	1.60E-07	0.68
Urea transmembrane transporter activity	Molecular function	15.55	1.77E-07	60
Urea transmembrane transport	Biological process	15.55	1.77E-07	60
Urea transport	Biological process	14.86	3.53E-07	50
Amide transmembrane transporter activity	Molecular function	12.47	3.84E-06	25
Amide transport	Biological process	12.42	4.04E-06	5.56
Water transmembrane transporter activity	Molecular function	12.21	4.99E-06	23.08
Integral component of plasma membrane	Cellular component	12.13	5.39E-06	1.40

astrocyte- enriched gene list (Figure 10B). Urea and amide transport genes were also enriched in altered genes, as well as water transport and membrane component genes (Figure 10B). The membrane component genes altered in the GO analysis overlap with many transporter genes altered in the microarray that reside in the membranes of astrocytes. Conditional deletion of *Atrx* by Cre recombinase driven by the *FoxG1* promoter results in complete deletion in the forebrain and therefore makes the effects of *Atrx* loss in one cell type, such as astrocytes, difficult to detect. To eliminate any cell non-autonomous effects from other cell types, a model that deletes *Atrx* specifically in astrocytes is required.

3.2 Creation of a novel mouse model deleting *Atrx* in astrocytes

To study the role of ATRX in astrocytes specifically, a new mouse model was required. *Atrx*^{f/WT} females were crossed with *Glast-Cre*^{ERT} males to generate inducible KO (*Atrx*^{f/Y}*Glast-Cre*^{ERT}) and control (*Atrx*^{WT/Y}*Glast-Cre*^{ERT}) males. Cre recombinase under the *Glast* promoter will delete *Atrx* in astrocytes specifically. Tamoxifen administration results in Cre recombinase translocation to the nucleus and recombination at any *loxP* sites present in the genome. To validate that tamoxifen successfully induces deletion of *Atrx* expression in astrocytes, preliminary tamoxifen injections were performed on 3 month old inducible knockout and control males. One week post-final injection, male mice were sacrificed and hippocampal tissue was harvested for mRNA isolation. qRT-PCR of *Atrx* demonstrated no detectable change in *Atrx* expression (Figure 11A). P10, the

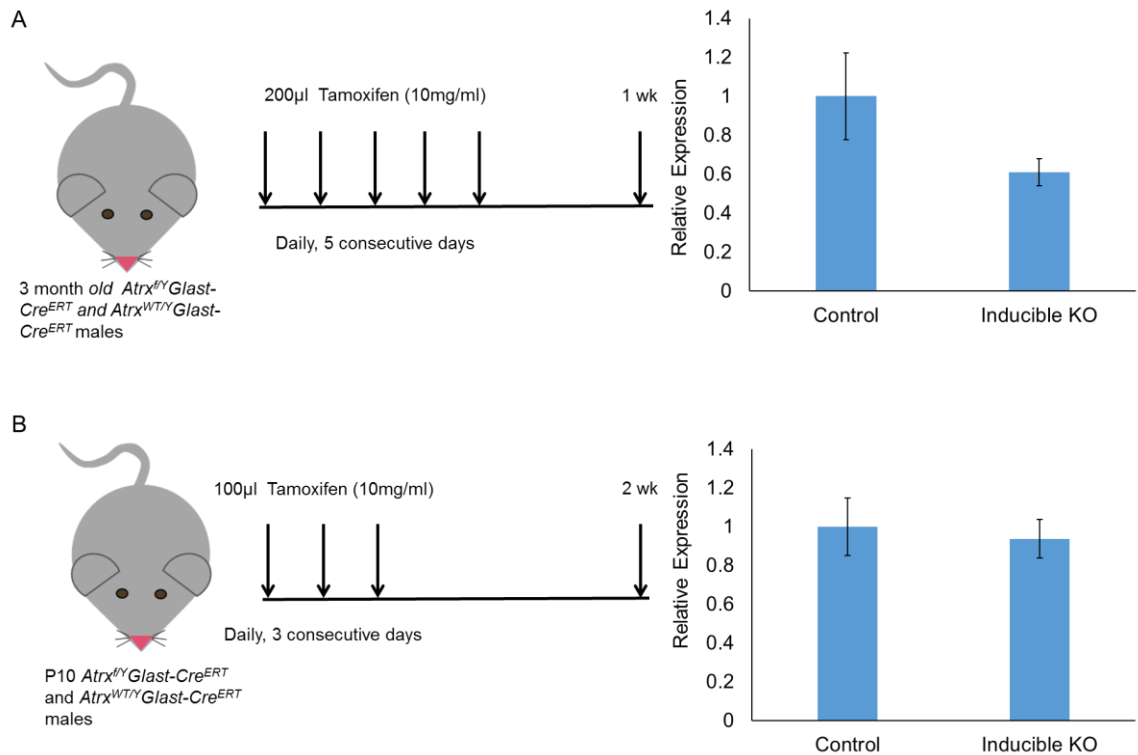


Figure 11. *Atrx* expression is not significantly decreased in the hippocampus of inducible knockout males. (A) Control and inducible knockout male mice were injected at 3 months of age for 5 consecutive days with 2 mg of tamoxifen. One week post-final injection, hippocampal RNA was isolated and mRNA levels of *Atrx* are not significantly decreased ($p=0.171$) (B) Control and inducible knockout males were injected at P10 for 3 consecutive days with 1 mg of tamoxifen. Two weeks post-final injection, hippocampal RNA was isolated and no detectable change between control and inducible KO was observed ($p=0.743$). Relative expression of *Atrx* was normalized to *Gapdh*. $n=3$.

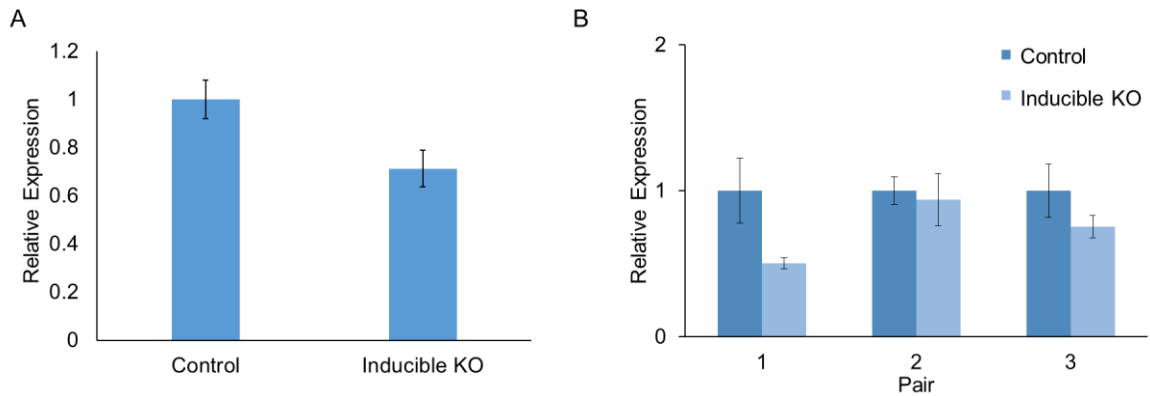
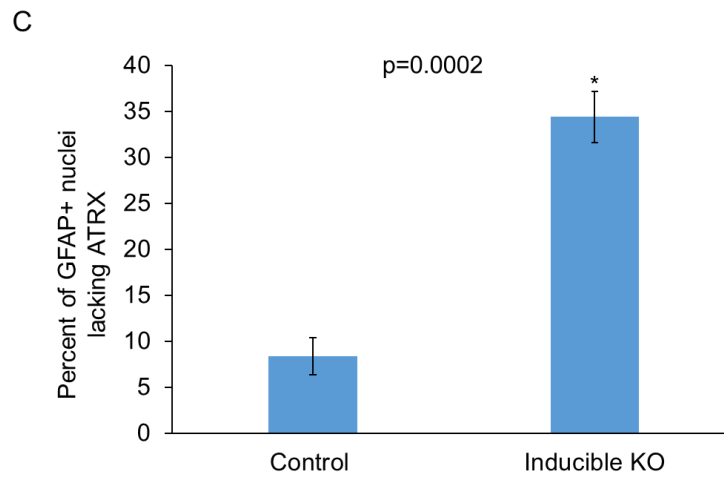
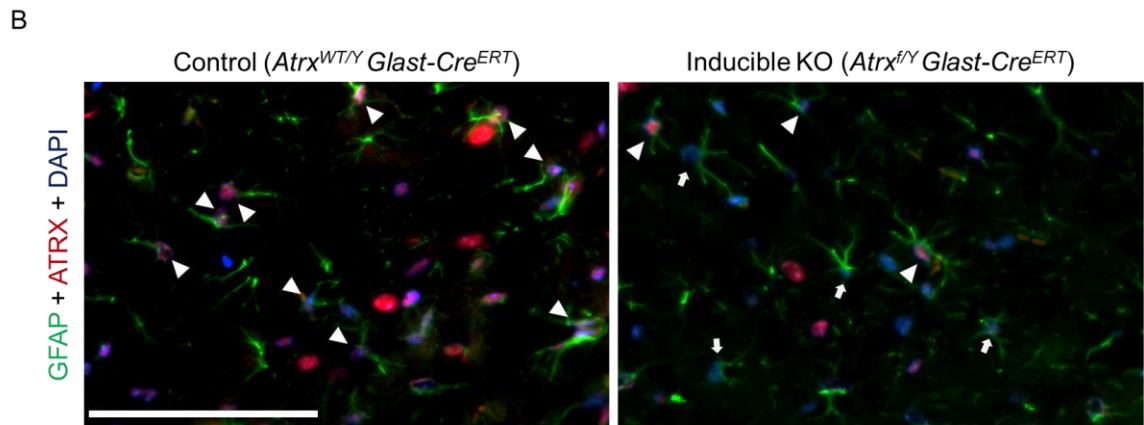
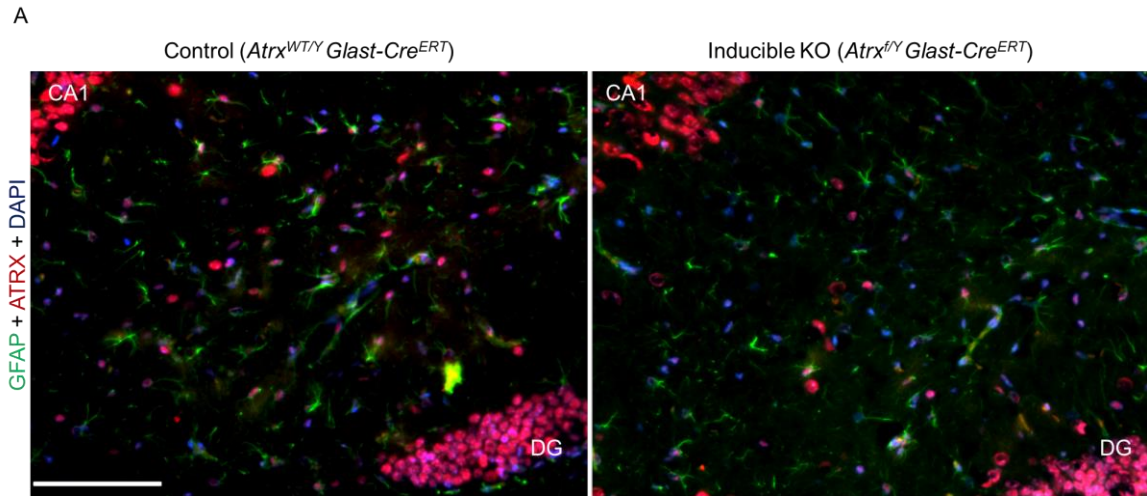


Figure 12. *Atrx* expression in the cortex of P26 control and inducible KO mice. (A) P26 cortical *Atrx* expression revealed no significant difference between 3 control and inducible KO pairs ($p=0.0584$). (B) Individual control and inducible KO pairs demonstrated variability in inducible KO *Atrx* expression after tamoxifen administration. Relative expression normalized to *Gapdh* expression. $n=3$.

injection start timepoint used throughout the rest of this work, control and inducible KO males were injected with tamoxifen for 3 consecutive days and sacrificed 2 weeks post-final injection at P26. Analysis of *Atrx* mRNA expression in the hippocampus of inducible KO revealed no detectable change from control levels (Figure 11B). *Atrx* mRNA levels were also measured in the cortex at P26 after P10 to P12 injection with tamoxifen. Although overall there is no significant change in average *Atrx* expression in the cortex of three pairs of control and inducible KO males (Figure 12A), if each pair is analyzed individually, there is variation in *Atrx* expression between pairs from different litters (Figure 12B). Pair 1 demonstrated decreased *Atrx* expression, however pair 2 displayed no change and pair 3 indicated a smaller decrease than pair 1 (Figure 12B). This variability between pairs contributed to no significant change being observed overall (Figure 12A). Overall, because *Atrx* is deleted in a subset of astrocytes and is still expressed in other cell types in the brain, detecting changes in *Atrx* by qRT-PCR is difficult. The expression of *Atrx* in neurons, oligodendrocytes and other cell types may be clouding any decrease in *Atrx* expression in astrocytes. Therefore, a different method, such as assessing whether ATRX is present in cells by immunofluorescence detection is required.

To validate that *Atrx* is being deleted specifically in astrocytes, cell counts were performed in a blinded manner on P26 control and inducible KO sagittal cryosections 2 weeks post-tamoxifen injection (Figure 13A). The sections were immunostained for GFAP, ATRX and DAPI. Three control and inducible KO males,

Figure 13. Percent of GFAP+ nuclei lacking ATRX is significantly increased in P26 hippocampus of inducible knockout compared to control. (A) Sagittal sections of control and inducible knockout hippocampi stained for GFAP (green), ATRX (red) and DAPI (blue). (B) Enlarged area of the hippocampus from (A). Arrowheads indicate GFAP positive cells expressing ATRX and full arrows indicate GFAP positive cells without ATRX staining. (C) Quantification of percent of GFAP positive nuclei that do not express ATRX. * indicates $p < 0.05$, $n = 3$. Scale bar = 100 μm



with one slide containing 3 sections for each of the 6 mice, were assessed. GFAP positive nuclei were counted, regardless of ATRX staining. Next, the GFAP positive but ATRX negative nuclei were counted in the same area. The number of GFAP positive nuclei lacking ATRX staining present in the hippocampus of inducible KO males was significantly higher when compared to controls (Figure 13C). An average of 34.4% of GFAP positive nuclei did not contain ATRX staining. Although ATRX is deleted in many GFAP-positive astrocytes (indicated by full arrows in Figure 13B), it is not deleted in all astrocytes, as indicated by arrowheads in Figure 13B. ATRX may be deleted in another astrocytes that do not express GFAP and therefore the deletion of ATRX in astrocytes may be more widespread than reported by GFAP and ATRX co-staining alone. *Glast-Cre^{ERT}* is also expressed in Bergmann glia in the cerebellum, and therefore ATRX staining in the cerebellum was also assessed. Immunostaining for GFAP, ATRX and DAPI was performed in the cerebellum of one P26 control and one inducible KO male. Many DAPI positive nuclei lacking ATRX staining were present in the inducible KO, where all nuclei in the control exhibited ATRX staining (Figure 14). Some of the ATRX-null nuclei are not surrounded by GFAP staining. These cells would require staining with another astrocyte marker to demonstrate they are indeed astrocytes. It is likely these nuclei lacking GFAP cytoplasmic staining are a different subtype of astrocyte expressing lower levels of GFAP. Overall, the ATRX staining in the cerebellum indicates that the *Glast-Cre^{ERT}* allows for Cre activation and

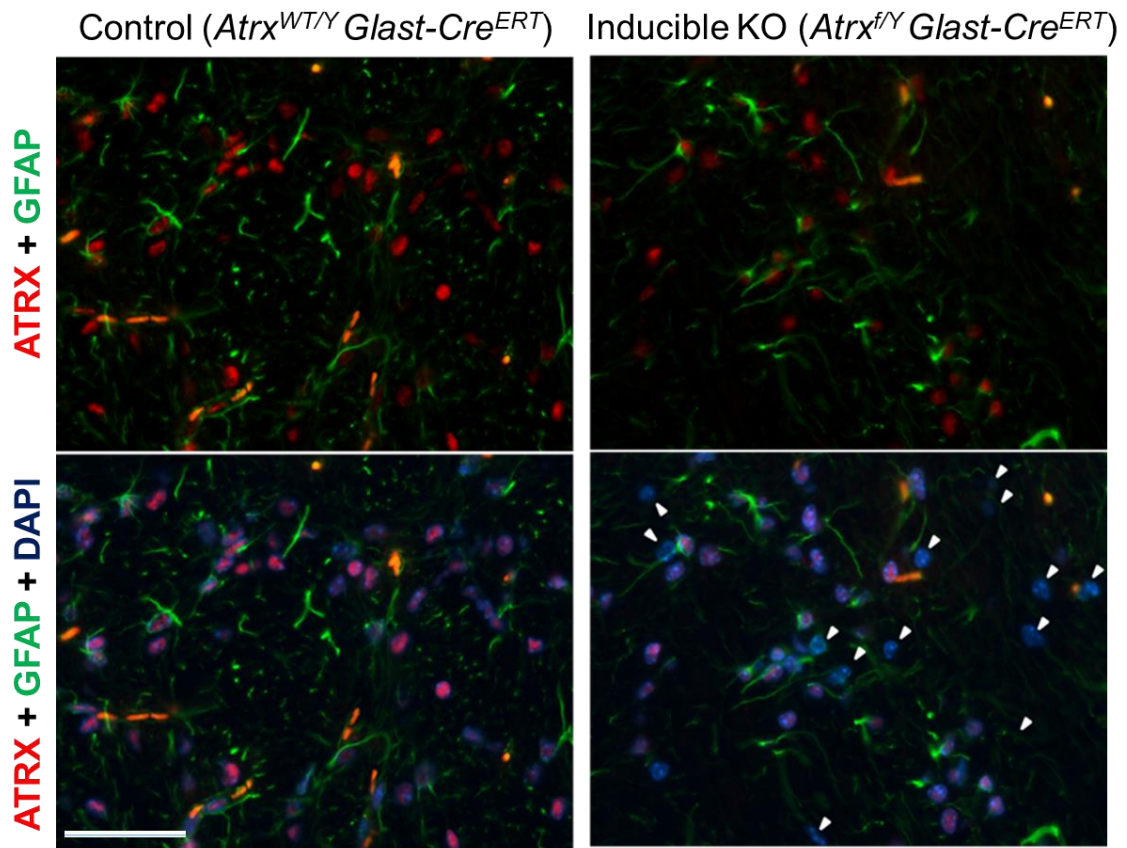


Figure 14. ATRX protein expression is decreased in cerebellum of P26 cerebellum of inducible KO. Sagittal sections of control and inducible KO hippocampi stained with GFAP (green), ATRX (red) and DAPI (blue) revealed DAPI positive nuclei lacking ATRX staining, as indicated by arrowheads. n=1. Scale bar=25 μ m.

recombination after tamoxifen administration.

GFAP does not label all astrocytes in the brain (Cahoy et al., 2008), and this makes visualization of *Atrx* deletion in astrocytes by immunofluorescence staining difficult. Therefore one copy of a double fluorescent reporter allele, *mT/mG^{WT/+}*, was crossed into the *Atrx^{f/WT}* female mice. The female mice carrying the double fluorescent reporter allele were crossed with *Glast-Cre^{ERT}* male mice to produce fluorescent control (*Atrx^{WT/Y}Glast-Cre^{ERT} mT/mG^{WT/+}*) and fluorescent inducible knockout (*Atrx^{f/Y}Glast-Cre^{ERT} mT/mG^{WT/+}*). The male mice will express GFP in astrocytes after Cre recombinase activation by tamoxifen. To ensure that GFP expression is specific to Cre recombinase activation by tamoxifen, male mice with and without the *Glast-Cre^{ERT}* but carrying a copy of the double fluorescent reporter allele (*Atrx^{WT/Y}mT/mG^{WT/+}* and *Atrx^{f/Y}Glast-Cre^{ERT} mT/mG^{WT/+}*, respectively) were injected from P10 to P12 and sacrificed 2 weeks post-final injection (at P26). One of these males (*Atrx^{WT/Y}mT/mG^{WT/+}*) does not contain Cre recombinase and therefore tamoxifen administration will not induce recombination and subsequent GFP expression from the double fluorescent reporter allele. The brains were sectioned sagittally and stained with DAPI to identify nuclei. The male lacking the *Glast-Cre^{ERT}* allele and carrying the *mT/mG* allele demonstrated no GFP expression after exposure to tamoxifen in both the cortex (Figure 15A) and hippocampus (Figure 15B). The male carrying the double reporter allele and the *Glast-Cre^{ERT}* allele demonstrated successful GFP induction (Figure 15A, B), indicating that tamoxifen administration is activating Cre recombinase activity.

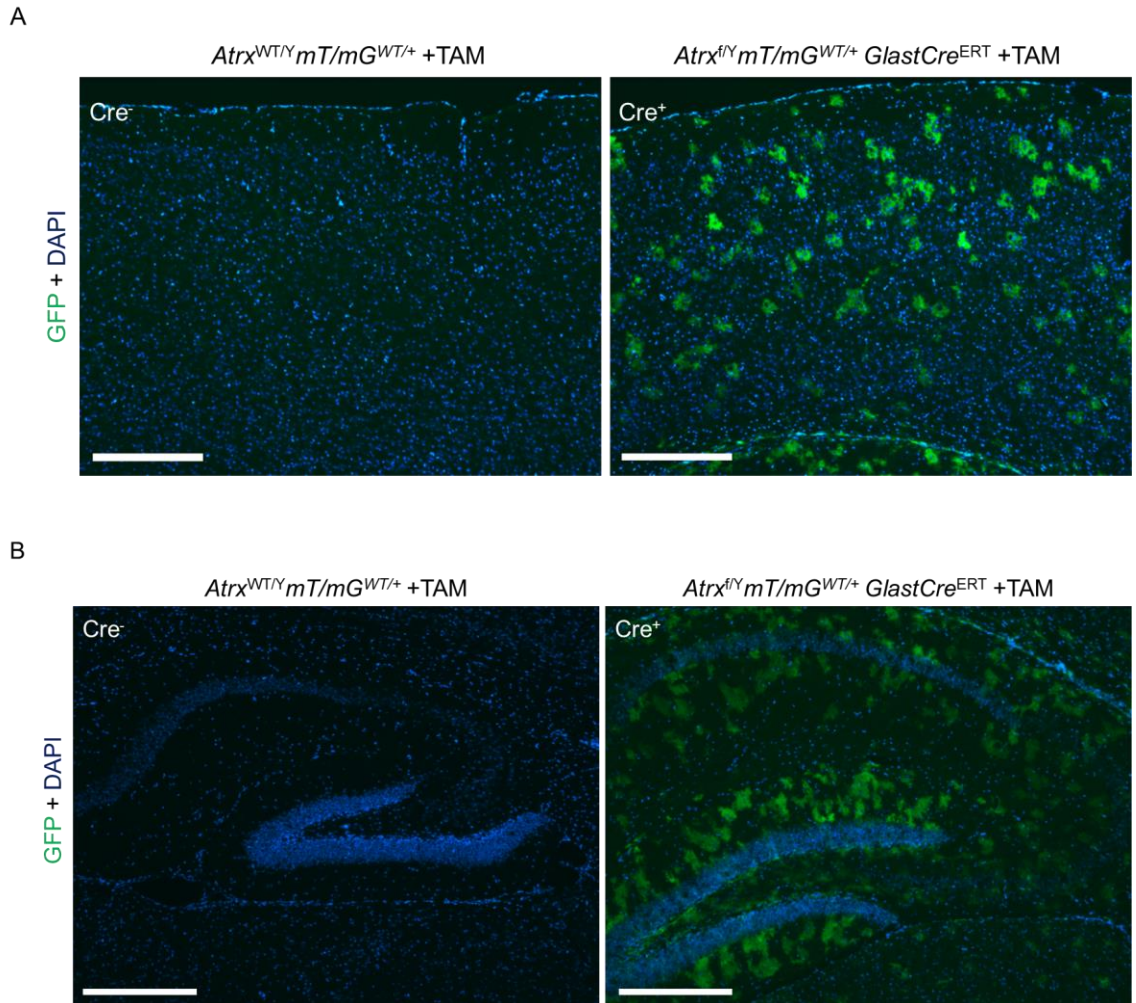


Figure 15. GFP expression in the cortex and hippocampus after tamoxifen administration in male mice carrying the *mT/mG* allele. (A) Sagittal sections of the cortex from males possessing both the *mT/mG* allele and with (right) or without (left) the *Glast-Cre*^{ERT} allele were stained with DAPI to reveal cytoplasmic GFP induction after tamoxifen administration only in the presence of the *Glast-Cre*^{ERT} allele. (B) Sagittal sections of the hippocampus from males possessing the *mT/mG* allele and with (right) or without (left) the *Glast-Cre*^{ERT} allele were stained with DAPI to reveal cytoplasmic GFP induction after tamoxifen administration only in the presence of the *Glast-Cre*^{ERT} allele. Scale bar=360 μ m.

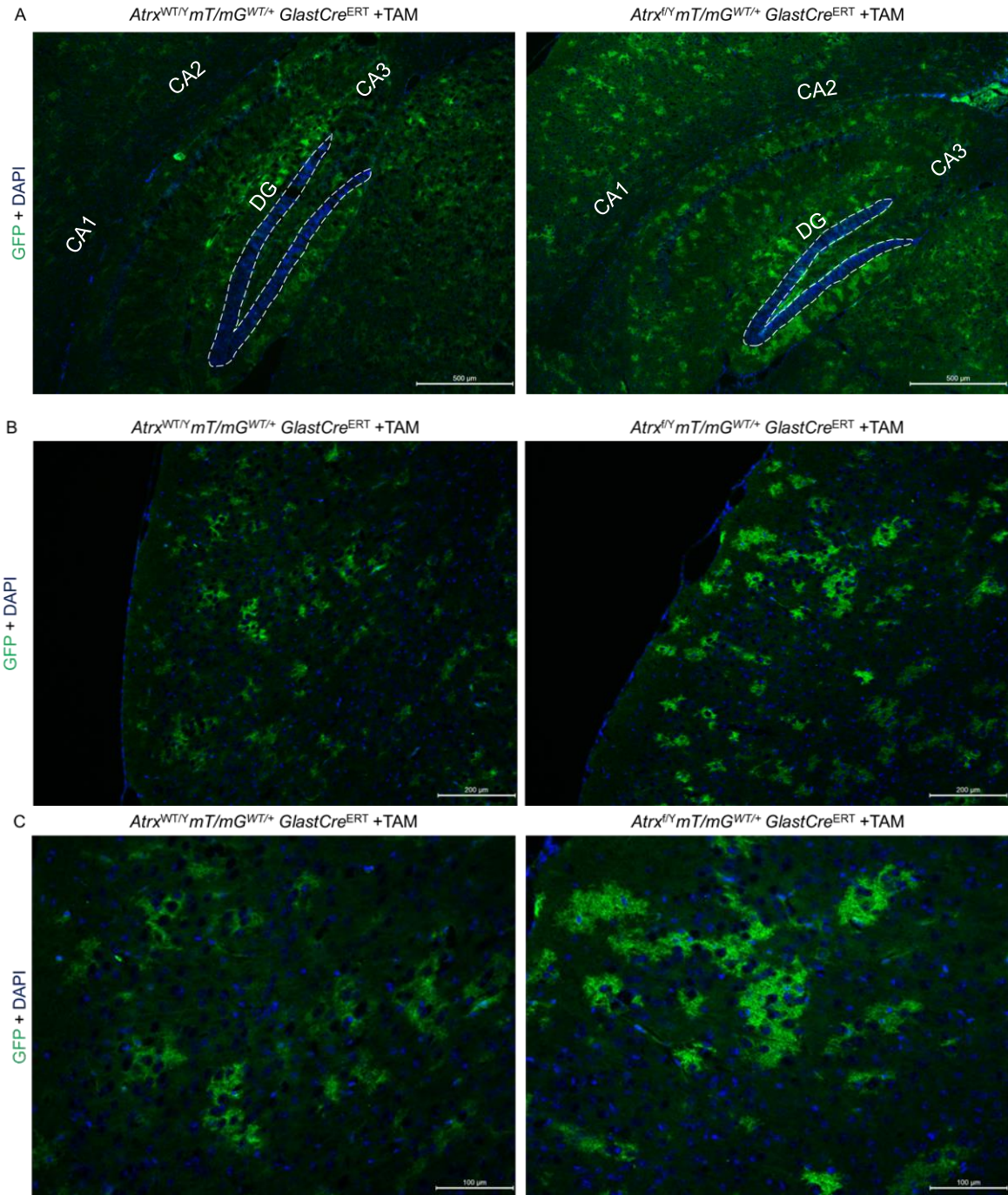
3.3 Preliminary morphological assessment of ATRX-null astrocytes

Astrocyte morphology can reflect astrocyte function. The cytoplasmic expression of GFP from the recombined *mT/mG* double reporter allele therefore provides an ideal system for studying morphology in astrocytes lacking *Atrx*. Astrocyte morphology was assessed after tamoxifen administration of control and inducible KO littermate pairs harbouring the *mT/mG* allele (Figure 5). Fluorescent control, *Atrx^{WT/Y}Glast-Cre^{ERT}mT/mG^{WT/+}*, and fluorescent inducible KO, *Atrx^{f/Y}Glast-Cre^{ERT}mT/mG^{WT/+}*, P26 sagittal cryosections were stained with DAPI and compared for GFP expression (Figure 16). The hippocampus of the fluorescent inducible KO demonstrated an increase in GFP domain number, however the astrocyte domain size appeared to be similar between fluorescent control and fluorescent inducible KO. *Glast-Cre^{ERT}* is also expressed in neural stem cell present in the dentate gyrus (Mori et al., 2006; Slezak et al., 2007), which is outlined in Figure 16A. GFP expression in this region was different when compared to the staining of hippocampal astrocytes (Figure 16A).

A striking increase in GFP domains in the cortex was demonstrated in fluorescent inducible KO compared to fluorescent control in the cortex (Figure 16B), indicating Cre recombinase expression is induced in more astrocytes. Astrocytic domains, visualized by GFP expression, also appeared larger in the fluorescent inducible KO, indicating larger astrocyte domains or more overlap between individual astrocyte domains (Figure 16C).

Morphological maturation is connected to molecular maturation and therefore expression of astrocyte maturation genes in the inducible KO should be assessed. To determine if loss of ATRX in astrocytes has an effect on astroglial maturation genes, qRT-PCR was performed on P26 (2 weeks post-injection) control and inducible knockout cortex. Relative expression of *connexin 30 (Gjb6)*, *connexin 43 (Gja1)* and glutamate transporter *Glut1 (Slc1a2)* revealed no significant change between control and inducible KO (Figure 17). However, Connexin 30 expression did appear decreased without reaching statistical significance. Increasing the number of biological replicates and assessing protein levels of connexin 30 will be required to clarify this result.

Figure 16. ATRX⁻ GFP⁺ astrocytes display altered morphology in the P26 cortex. (A) GFP expression was induced in the hippocampus of fluorescent control (*Atrx*^{WT/Y}*mT/mG*^{WT/+} *GlastCre*^{ERT}) and fluorescent inducible KO (*Atrx*^{f/Y}*mT/mG*^{WT/+} *GlastCre*^{ERT}). Expression of GFP was also in neural stem cells in outlined dentate gyrus. Scale bar= 500 μm (B) GFP was expressed in more astrocytes, giving rise to more GFP positive domains, in the inducible KO cortex. Domains also appear larger in fluorescent inducible KO compared to fluorescent control. Scale bar= 200 μm. (C) Higher magnification of GFP domains revealed larger domains with higher intensity of GFP expression in fluorescent inducible KO. Scale bar= 100 μm.



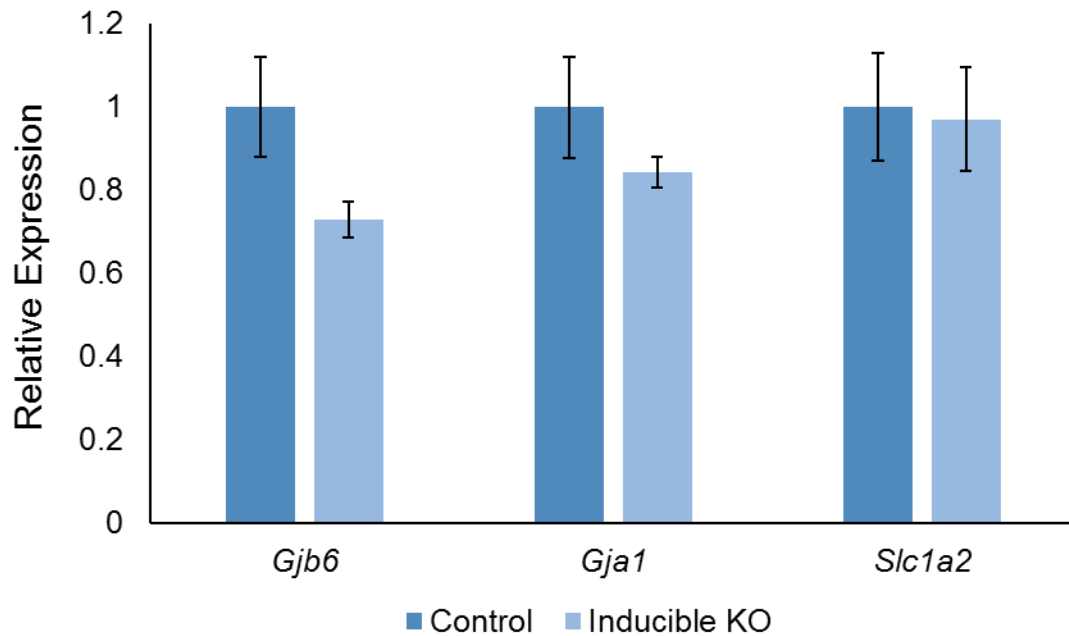


Figure 17. Expression analysis of astroglial genes in the P26 cortex of control and inducible KO mice. Analysis of control and inducible KO cortical transcript levels at 2 weeks post-injection (P26) revealed no significant change in *connexin 30* (*Gjb6*) ($p=0.101$), *connexin 43* (*Gja1*) ($p=0.287$) and *Glt1* (*Slc1a2*) ($p=0.876$). Relative expression normalized to *Gapdh* expression. $n=3$.

4 Discussion

4.1 Loss of ATRX in the forebrain affects the astrocyte population

4.1.1 *Aldh1l1* expression and the number of astrocytes present in the cKO is variable

The deletion of *Atrx* beginning at E8.5 in the forebrain by Cre recombinase driven by the *Foxg1* promoter resulted in p53-mediated apoptosis of neuroprogenitors and microcephaly in the mouse brain (Berube *et al.*, 2005; Ritchie *et al.*, 2014; Seah *et al.*, 2008). It is well established that ATRX is required for maintenance of the neuroprogenitor pool and its loss causes sensitivity to replicative stress (Ritchie *et al.*, 2014; Watson *et al.*, 2013). However, the effects on the astrocyte population remain unclear. The increased amount of neuroprogenitor cell death in the embryonic brain of the cKO indicates that astrocytes may respond by becoming reactive (Sofroniew and Vinters, 2010). Astrocytes are not generated until after birth (Yang *et al.*, 2013), however the cell death observed in the neuroprogenitor population occurs embryonically (Berube *et al.*, 2005; Seah *et al.*, 2008; Watson *et al.*, 2013). Reactive astrocytes may remain reactive to block off damage in the brain (Sofroniew and Vinters, 2010). Assessment of immunofluorescent staining for GFAP in the hippocampus revealed an increase in 2 pairs of P7 control and cKO coronal sections (Figure 7). It is possible that GFAP staining would be higher closer to birth, after the first astrocytes are born and begin to react to their environment.

Quantitative analysis of GFAP by western blot revealed no significant change in the expression of this astrocyte-specific marker (Figure 8A, B). However, the possibility of whether there was a decrease in the number of astrocytes in the cKO needed to be addressed. Although the protein levels of Aldh1l1, a more global astrocyte-specific marker (Cahoy *et al.*, 2008), did not show significant change between control and cKO when averaged between three pairs, variability was observed in the western blot (Figure 8A). Pairs 1 and 2 showed a decrease in the expression of Aldh1l1 in cKOs compared to controls, but pair 3 did not show the same trend (Figure 8A). To determine whether this decrease in Aldh1l1 was due to decreased protein expression per cell or a decrease in the astrocyte population overall (Figure 9A), cell counts of Aldh1l1 positive cells in the cortex of three control and cKO pairs were performed and also revealed inconsistencies between pairs (Figure 9B): two pairs demonstrated a decrease in astrocytes number in the cKO and one pair displayed the opposite result. Immunostaining also revealed decreased intensity of Aldh1l1 staining in the cKO, indicating there may be decreased levels of Aldh1l1 per astrocyte (Figure 9C). The biological variability in these experiments is likely a result ATRX loss in these cells. If there were less astrocytes in the cKO forebrain, GFAP levels may be increased per astrocyte as there was an increase (nonsignificant) in the cKO males (Figure 8B). Indeed, when GFAP protein levels were normalized to Aldh1l1, GFAP levels were increased, however this increase was still not statistically significant (Figure 8C). Analysis of additional mice might help to determine if astrocyte number is consistently decreased and if there is a higher number of reactive astrocytes in the cKO. This

could result in altered astrocyte function in the cKO brain as reactive astrocytes alter their gene expression to contain damage and inflammation, thereby neglecting normal functions (Zamanian *et al.*, 2012). These results are, however, variable between control and cKO pairs. A better model to study ATRX inactivation in astrocytes, without cell non-autonomous effects, was required and is discussed further in section 4.2.

4.1.2 *ATRX loss in the embryonic forebrain results in altered expression of astrocytes enriched genes.*

A microarray assessing altered gene expression in control and cKO was previously performed in our lab (unpublished, Michael Levy). The analysis of microarray data at P17 indicated that many astrocyte-enriched genes exhibited altered expression, based on microarray binding intensities, in the ATRX-null forebrain. (Figure 10A). The top 3 downregulated genes were all decreased by approximately 1.6 to 2-fold. *Aqp4* was the most altered astrocyte-enriched gene and was downregulated 2-fold in the cKO forebrain. AQP4 channels are present at the endfeet of astrocytes and make contacts with the blood brain barrier and the barriers of cerebral spinal fluid vessels (Amiry-Moghaddam and Ottersen, 2003; Gomes *et al.*, 2009). They also colocalize with potassium channel Kir4.1 at the membrane of astrocytic endfeet and PAPs, assisting with potassium transport by concentration gradient regulation in the brain (Amiry-Moghaddam and Ottersen, 2003; Gomes *et al.*, 2009). Deletion of *Aqp4* in glia resulted in reduced water absorption at the blood-brain barrier, but did not increase permeability to macromolecules (Haj-Yasein *et al.*, 2011). AQP4 is important in regulating the extracellular space of synapses during excitatory

synaptic transmission in the brain (Haj-Yasein *et al.*, 2012). This decrease in *Aqp4* could affect synaptic function in the cKO brain and overall water and potassium homeostasis.

Dio2 was the second most downregulated gene in the cKO P17 forebrain. DIO2 is the enzyme responsible for converting thyroxine (T4) into the active thyroid hormone triiodothyronine (T3) and its expression takes place predominantly in glial cells, specifically in astrocytes (Morte and Bernal, 2014). Astrocytes can take up circulating T4 from the blood through their connections with the blood brain barrier and T4 can be converted to T3 through DIO2-mediated deiodination (Morte and Bernal, 2014). This decrease in *Dio2* could lead to decreased T3 production in the brain. T3 is important for brain development and has been linked to neuronal migration, synaptogenesis and myelination (Preau *et al.*, 2015). Interestingly, cKO have decreased serum T4 levels (Watson *et al.*, 2013) and also exhibit decreased levels of myelin proteins at P20 (Matthew Edwards, unpublished). Given that astrocytes are responsible for converting T4 to T3 through DIO2, they may play a role in the myelination defects observed in cKO males.

Tnc was downregulated to a similar degree as *Dio2*. TNC is an astrocyte-secreted molecule that is involved in extracellular matrix remodeling after brain injury and in synaptic plasticity and axonal guidance during brain development (Jones and Bouvier, 2014). TNC can promote or inhibit synapse formation during development, depending on other signals present (Jones and Bouvier, 2014). TNC-null mice exhibited high neuronal density, increased reactive astrogliosis, and reduced LTP in the hippocampus (Evers *et al.*, 2002; Irintchev *et al.*, 2005). *Tnc*

expression decreases in the adult brain after development but an increase in its expression is correlated with the induction of reactive astrocytes (Jones and Bouvier, 2014). In fact, GFAP levels were significantly lower in TNC-null reactive astrocytes when compared to wildtype and inflammatory cytokine levels were also altered (Ikeshima-Kataoka *et al.*, 2008). Therefore, if *Tnc* is downregulated in the cKO, this could impact synaptogenesis as well as how astrocytes respond to injury or inflammation. This decrease in *Tnc* expression could also result in GFAP not being upregulated to its full extent in reactive astrocytes, yielding an insignificant change in protein levels observed in Figure 8.

GO analysis identified enriched pathways in altered genes. The majority of altered pathways involved homeostatic functions, such as urea transport and water transport performed by astrocytes (Figure 10B). Integral and intrinsic membrane components were also enriched in altered genes and this refers to the many transporters and channels present on the membrane of astrocytes that are altered in the cKO. Taken together, the results suggest homeostatic functions of astrocytes are altered in the cKO, contributing to pathology in the brain.

4.2 Creation of a novel mouse model

To further study the role of ATRX in astrocytes, Cre recombinase driven by an astrocyte-specific promoter was required to delete *Atrx*. To accomplish this, a cross between *Atrx*^{f/WT} females and males carrying the *Glast-Cre*^{ERT} allele was performed. This Cre recombinase is activated by tamoxifen administration, causing recombination of the floxed *Atrx* allele in astrocytes. This model also

allows for temporal control of *Atrx* deletion in astrocytes. Efficient recombination of the floxed *Atrx* gene was difficult to detect as qRT-PCR analysis of *Atrx* expression in the hippocampus could not detect a significant decrease in the inducible KO at 3 months of age (Figure 11A). This difficulty can be explained by all other cell types still expressing *Atrx* in the inducible KO and the small change in astrocyte-specific *Atrx* expression is undetectable as a result of the high expression of the gene in other cell types. A more effective approach will be to use a fluorescent reporter allele that is activated by *Glast-Cre^{ERT}* to purify control and inducible KO astrocytes with fluorescence-activated cell sorting (FACs). This will provide a relatively pure astrocyte populations and deletion of *Atrx* would be detectable in males carrying the floxed *Atrx* allele.

Previous studies identified ATRX as important for neuroprogenitor survival when ATRX was deleted embryonically (Berube *et al.*, 2005; Ritchie *et al.*, 2014; Seah *et al.*, 2008; Watson *et al.*, 2013). Given the importance of ATRX in proliferating cells, injection during peak astrogliogenesis was avoided as to not induce replication, DNA damage, and apoptosis in astrocytes. Instead, control and inducible KO males began injections at P10, and ended at P12, as peak astrogliogenesis ends at approximately P7 (Yang *et al.*, 2013). *Atrx* mRNA levels were not significantly decreased in the hippocampus (Figure 11B). Tamoxifen injections may cause variability in Cre recombinase induction if one male receives less tamoxifen than another due to human error. Also, the brain is smaller at P26 as it is developing and hippocampal dissection is difficult. It is possible that the high expression of *Atrx* in neurons may shield any decrease in astrocytes from

being observed. More tamoxifen treated control and inducible KO pairs must be assessed to determine if there is a detectable. qRT-PCR performed on P26 control and inducible cortex also demonstrated no significant change in average expression in three pairs (Figure 12A). If each pair is analyzed individually, however, it is clear that there is variability in *Atrx* expression (Figure 12B). Pair 1 exhibited a significant decrease in *Atrx* levels by approximately 50% and Pair 3 also showed a decrease in inducible KO, however not to the same extent. Pair 2 demonstrated no change in *Atrx* levels between control and inducible KO. This variability could be due to different tamoxifen levels reaching the brain after injection. To determine whether this decrease in the cortex is consistent, more biological replicates must be performed to rule out any technical issues with tamoxifen delivery via intraperitoneal injection. Also a FACs experiment, as mentioned in the above paragraph, could be used to isolate the astrocyte population and assess the deletion of *Atrx* at this timepoint.

The protein levels of ATRX in astrocytes revealed that an average of 34.4% of GFAP positive nuclei lacked ATRX staining in a selected area of the hippocampus (Figure 13C). It is important to note that GFAP does not stain all astrocytes (Figure 13A, B) and therefore this may underestimate the recombination efficiency. Immunostaining in the cerebellum also revealed nuclei lacking ATRX staining, some surrounded by cytoplasmic GFAP staining and some not (Figure 14). These ATRX-deficient nuclei lacking GFAP staining could indicate that another subtype of astrocyte, which does not express GFAP at detectable levels, expressed Cre recombinase in response to tamoxifen. One major challenge in the field is a lack

of a nuclear astrocyte marker, and the heterogeneity of astrocytes makes cytoplasmic marker ALDH1L1 the best candidate for labeling the most astrocytes (Cahoy *et al.*, 2008). Cell counts in the cortex after tamoxifen injection should therefore be performed using an anti-Aldh1l1 antibody. This will allow for validation of ATRX deletion at the protein level in the cortex. A double reporter allele, however, was used to track Cre recombinase induction after tamoxifen injection. This allele expressed GFP after Cre recombinase-mediated recombination, and therefore after tamoxifen treatment in astrocytes in this model. Figure 15 demonstrates that GFP expression is only observed in the presence of the *Glast-Cre^{ERT}* allele, indicating that tamoxifen is reaching the brain and inducing recombination. This also shows that tamoxifen can cross the blood brain barrier successfully and bind the estrogen receptor-fused Cre recombinase, allowing for its translocation to the nucleus.

4.3 Altered morphology and decreased expression of gap junction protein in inducible KO

4.3.1 *Increase in number of astrocytes undergoing recombination and altered morphology in the cortex at P26 in inducible KO*

Through use of a double reporter allele, astrocyte domains and morphology were assessed in *Atrx^{WT/Y}Glast-Cre^{ERT}mT/mG^{WT/+}* and *Atrx^{f/Y}Glast-Cre^{ERT}mT/mG^{WT/+}* mice. Interestingly, in both the hippocampus and cortex of the fluorescent inducible KO there was an increase in the number of GFP domains (Figure 16A), which represent astrocyte domains as the GFP in the double reporter allele is membrane targeted (Muzumdar *et al.*, 2007). The increase in GFP positive domains indicates

more astrocytes being exposed to tamoxifen at the blood brain barrier. It is important to note that before tamoxifen injection, the fluorescent control and inducible KO have the same gene expression as *Atrx* will not be deleted in astrocytes until after tamoxifen exposure. The injection protocol for these mice was 3 consecutive, daily injections from P10 to P12 (Figure 11B). After the first injection, the permeability of astrocytes lacking *Atrx* to tamoxifen at the blood brain barrier may increase, leading to more astrocytes taking up tamoxifen from the blood in the daily injections that follow. Investigation as to why more astrocytes carrying the *Atrx*-floxed allele undergo recombination after tamoxifen administration is required to understand the mechanism of how ATRX loss may affect permeability of astrocytes to tamoxifen.

In the cortex, the fluorescent inducible KO exhibited larger GFP positive domains (Figure 16B, C). This could indicate that 1) astrocyte morphology is altered such that individual astrocyte domains are larger in the inducible KO, 2) there is more overlap between individual astrocyte domains, or 3) a combination of the two. Because the GFP expressed from the double reporter allele is membrane targeted, it is difficult to distinguish if the large GFP domain is from one or multiple nuclei. Therefore if the large domains result from astrocytes having expanded PAPs, this could indicate a defect in morphological maturation. Astrocytes lacking ATRX do not respond to development cues that result in the pruning of their PAPs by 4 weeks of age (Yang *et al.*, 2013). This is also a possibility if the large GFP positive domains are caused by an overlap of multiple astrocytes. Astrocytes should retreat to non-overlapping domains by P28 (Yang *et al.*, 2013). The timepoint analyzed

was P26 and therefore most astrocytes should occupy their own respective domains. The apparent domain expansion might be caused by a combination of increased astrocyte domain coverage and overlap between astrocytes. This morphology defect could be caused by delay in astrocyte morphological maturation due to ATRX loss or the permanent inability for ATRX-null astrocyte to prune their excess PAPs. To assess if this phenotype is permanent or a delay in development, the mutant mice should be assessed a month post-tamoxifen injection. If the phenotype persists, one could conclude that ATRX-null astrocytes have lost their ability to occupy specific domains.

Regardless of whether this phenotype is a delay in maturation or a permanent increase in astrocyte domain size, it is clear that there are implications for synaptogenesis and synaptic plasticity. The timing of synaptogenesis overlaps with astrocyte morphological maturation (Figure 2). Astrocytes release factors that help with the pruning of unnecessary synapses during development (Bialas and Stevens, 2013). If astrocytes have enlarged domains, it is likely that they are making more connections with synapses. This could lead to decreased synaptic pruning if astrocytes themselves are not pruning PAPs during development. Assessment of TNF- β levels, the signal secreted from astrocytes to initiate synaptic refinement, should be assessed in the future. Dendrite morphology of neurons through Golgi staining would also provide insight as to whether synaptic refinement has taken place in the cortex of the inducible KO.

If this phenotype is permanent, it has implications for synaptic plasticity in memory and learning after development. Astrocytes can help strengthen synapses during

a learning event by adjusting PAPs to contact synapses undergoing stimulation (Bernardinelli *et al.*, 2014). The mobility of astrocytic PAPs is important to allow for selective contacts with synapses (Bernardinelli *et al.*, 2014). If astrocytes cannot prune excess PAPs during development, they may also be unable to undergo PAP plasticity to reach and strengthen stimulated synapses in the adult brain. Further investigation is required to understand if astrocytes lacking ATRX retain structural plasticity, and more importantly if the enlarged astrocyte domains remain at later timepoints. Confocal microscopy and a primary antibody labeling GFP would enable better visualization of fine PAPs.

4.3.2 *Change in connexin 30 (Gjb6) expression in cortex of inducible KO at P26*

A nonsignificant decrease in *connexin 30 (Gjb6)* expression was observed at P26 in the cortex of the inducible KO when compared to control (Figure 17). This decrease will need to be verified in a pure astrocyte population after using FACs to sort out control and inducible KO astrocytes. Western blot analysis of GJB6 protein levels between control and inducible KO should be performed to determine if there is a significant decrease in the gap junction protein. If there is indeed a decrease in GJB6, there are many implications to astrocyte morphology and function. GJB6 and GJA1 make up gap junctions present in astrocytes and allow for intercellular communications between astrocytes (Pannasch and Rouach, 2013). These connections allow for efficient mediation of brain homeostasis through ion buffering and nutrient transport (Pannasch and Rouach, 2013). GJB6 controls excitatory synaptic transmission in the hippocampus and does so by

mediating morphological changes that insert the astrocytic PAPs into synaptic clefts where glutamate transport can be more finely regulated (Pannasch *et al.*, 2014). GJB6-null mice have larger astrocytic domain with elongated processes and increased branching (Pannasch *et al.*, 2014), a phenotype similar to the morphological changes observed in the fluorescent inducible KO. Loss of *Gjb6* also resulted in increased insertion of PAPs into synaptic clefts and altered excitatory transmission at the synapse (Pannasch *et al.*, 2014). Therefore the decrease in *Gjb6* expression in our mouse model could play a role in the morphological changes observed in ATRX-deficient astrocytes.

Conclusions and future directions

This study was initiated to address the potential functions of ATRX in astrocytes. We found that deletion of ATRX in all cells in the forebrain affected the astrocyte population by increasing the amount of reactive astrocytes. The results, however, were variable and firm conclusions could not be made. ATRX loss likely affects the number of astrocytes in the brain, as well as increasing their reactivity. More biological replicates are required to establish the consistency of these phenotypes. Analysis of microarray expression between control and cKO revealed ATRX deletion affects the expression of astrocyte-specific genes and pathways.

A novel mouse model was created utilizing an inducible Cre recombinase under the control of an astrocyte-specific promoter. This Cre recombinase responds to tamoxifen administration, causing recombination of the floxed *Atrx* allele specifically and temporally in astrocytes. The use of a double reporter allele

revealed enlarged and possibly overlapping astrocyte domains in ATRX mutant mice compared to controls. This morphological change was accompanied by a potential decrease in expression of *Cx30*, a key component of astrocyte gap junctions. Further analysis of connexin 30 expression at both the mRNA and protein level is required to determine if deletion of *Atrx* results in its decreased expression.

The extent of ATRX inactivation on gene expression in astrocytes must be investigated further to understand the phenotypes observed above. Future directions for this study include assessing gene expression changes in ATRX-null astrocytes. Fluorescence-activated cell sorting could be used to isolate astrocytes and subsequent RNA sequencing would reveal changes between control and inducible KO. This would provide more insight into defects caused by ATRX loss in astrocytes. Another important question to answer involves whether ATRX-null astrocytes can support the growth and development of neurons, which could be addressed in co-culture experiments. Behavioural analysis of inducible KO mice would indicate whether ATRX is required in astrocytes for proper learning and memory. These experiments will indicate as to whether ATRX loss in astrocytes is contributing to the pathology experienced in the brains of individuals with ATR-X syndrome.

References

- Aapola, U., Kawasaki, K., Scott, H.S., Ollila, J., Vihinen, M., Heino, M., Shintani, A., Kawasaki, K., Minoshima, S., Krohn, K., *et al.* (2000). Isolation and initial characterization of a novel zinc finger gene, DNMT3L, on 21q22.3, related to the cytosine-5-methyltransferase 3 gene family. *Genomics* 65, 293-298.
- Allen, N.J., Bennett, M.L., Foo, L.C., Wang, G.X., Chakraborty, C., Smith, S.J., and Barres, B.A. (2012). Astrocyte glypicans 4 and 6 promote formation of excitatory synapses via GluA1 AMPA receptors. *Nature* 486, 410-414.
- Amir, R.E., Van den Veyver, I.B., Wan, M., Tran, C.Q., Francke, U., and Zoghbi, H.Y. (1999). Rett syndrome is caused by mutations in X-linked MECP2, encoding methyl-CpG-binding protein 2. *Nature genetics* 23, 185-188.
- Amiry-Moghaddam, M., and Ottersen, O.P. (2003). The molecular basis of water transport in the brain. *Nature reviews Neuroscience* 4, 991-1001.
- Anthony, T.E., Klein, C., Fishell, G., and Heintz, N. (2004). Radial glia serve as neuronal progenitors in all regions of the central nervous system. *Neuron* 41, 881-890.
- Araque, A., Carmignoto, G., Haydon, P.G., Oliet, S.H., Robitaille, R., and Volterra, A. (2014). Gliotransmitters travel in time and space. *Neuron* 81, 728-739.
- Ballas, N., Lioy, D.T., Grunseich, C., and Mandel, G. (2009). Non-cell autonomous influence of MeCP2-deficient glia on neuronal dendritic morphology. *Nature neuroscience* 12, 311-317.
- Belanger, M., Allaman, I., and Magistretti, P.J. (2011). Brain energy metabolism: focus on astrocyte-neuron metabolic cooperation. *Cell metabolism* 14, 724-738.
- Bernardinelli, Y., Randall, J., Janett, E., Nikonenko, I., Konig, S., Jones, E.V., Flores, C.E., Murai, K.K., Bochet, C.G., Holtmaat, A., *et al.* (2014). Activity-dependent structural plasticity of perisynaptic astrocytic domains promotes excitatory synapse stability. *Current biology : CB* 24, 1679-1688.
- Berube, N.G. (2011). ATRX in chromatin assembly and genome architecture during development and disease. *Biochemistry and cell biology = Biochimie et biologie cellulaire* 89, 435-444.
- Berube, N.G., Jagla, M., Smeenk, C., De Repentigny, Y., Kothary, R., and Picketts, D.J. (2002). Neurodevelopmental defects resulting from ATRX overexpression in transgenic mice. *Human molecular genetics* 11, 253-261.

Berube, N.G., Mangelsdorf, M., Jagla, M., Vanderluit, J., Garrick, D., Gibbons, R.J., Higgs, D.R., Slack, R.S., and Picketts, D.J. (2005). The chromatin-remodeling protein ATRX is critical for neuronal survival during corticogenesis. *The Journal of clinical investigation* 115, 258-267.

Berube, N.G., Smeenk, C.A., and Picketts, D.J. (2000). Cell cycle-dependent phosphorylation of the ATRX protein correlates with changes in nuclear matrix and chromatin association. *Human molecular genetics* 9, 539-547.

Bialas, A.R., and Stevens, B. (2013). TGF-beta signaling regulates neuronal C1q expression and developmental synaptic refinement. *Nature neuroscience* 16, 1773-1782.

Bushong, E.A., Martone, M.E., and Ellisman, M.H. (2004). Maturation of astrocyte morphology and the establishment of astrocyte domains during postnatal hippocampal development. *International journal of developmental neuroscience : the official journal of the International Society for Developmental Neuroscience* 22, 73-86.

Caceres, M., Suwyn, C., Maddox, M., Thomas, J.W., and Preuss, T.M. (2007). Increased cortical expression of two synaptogenic thrombospondins in human brain evolution. *Cerebral cortex* 17, 2312-2321.

Cahoy, J.D., Emery, B., Kaushal, A., Foo, L.C., Zamanian, J.L., Christopherson, K.S., Xing, Y., Lubischer, J.L., Krieg, P.A., Krupenko, S.A., *et al.* (2008). A transcriptome database for astrocytes, neurons, and oligodendrocytes: a new resource for understanding brain development and function. *The Journal of neuroscience : the official journal of the Society for Neuroscience* 28, 264-278.

Christopherson, K.S., Ullian, E.M., Stokes, C.C., Mallowney, C.E., Hell, J.W., Agah, A., Lawler, J., Mosher, D.F., Bornstein, P., and Barres, B.A. (2005). Thrombospondins are astrocyte-secreted proteins that promote CNS synaptogenesis. *Cell* 120, 421-433.

Clynes, D., Jelinska, C., Xella, B., Ayyub, H., Taylor, S., Mitson, M., Bachrati, C.Z., Higgs, D.R., and Gibbons, R.J. (2014). ATRX dysfunction induces replication defects in primary mouse cells. *PloS one* 9, e92915.

De La Fuente, R., Viveiros, M.M., Wigglesworth, K., and Eppig, J.J. (2004). ATRX, a member of the SNF2 family of helicase/ATPases, is required for chromosome alignment and meiotic spindle organization in metaphase II stage mouse oocytes. *Developmental biology* 272, 1-14.

Dhayalan, A., Tamas, R., Bock, I., Tattermusch, A., Dimitrova, E., Kudithipudi, S., Ragozin, S., and Jeltsch, A. (2011). The ATRX-ADD domain binds to H3 tail peptides and reads the combined methylation state of K4 and K9. *Human molecular genetics* 20, 2195-2203.

Dolce, A., Ben-Zeev, B., Naidu, S., and Kossoff, E.H. (2013). Rett syndrome and epilepsy: an update for child neurologists. *Pediatric neurology* 48, 337-345.

Drane, P., Ouararhni, K., Depaux, A., Shuaib, M., and Hamiche, A. (2010). The death-associated protein DAXX is a novel histone chaperone involved in the replication-independent deposition of H3.3. *Genes & development* 24, 1253-1265.

Emsley, J.G., and Macklis, J.D. (2006). Astroglial heterogeneity closely reflects the neuronal-defined anatomy of the adult murine CNS. *Neuron glia biology* 2, 175-186.

Eustermann, S., Yang, J.C., Law, M.J., Amos, R., Chapman, L.M., Jelinska, C., Garrick, D., Clynes, D., Gibbons, R.J., Rhodes, D., *et al.* (2011). Combinatorial readout of histone H3 modifications specifies localization of ATRX to heterochromatin. *Nature structural & molecular biology* 18, 777-782.

Evers, M.R., Salmen, B., Bukalo, O., Rollenhagen, A., Bosl, M.R., Morellini, F., Bartsch, U., Dityatev, A., and Schachner, M. (2002). Impairment of L-type Ca²⁺ channel-dependent forms of hippocampal synaptic plasticity in mice deficient in the extracellular matrix glycoprotein tenascin-C. *The Journal of neuroscience : the official journal of the Society for Neuroscience* 22, 7177-7194.

Fakhoury, M. (2015). Autistic spectrum disorders: A review of clinical features, theories and diagnosis. *International journal of developmental neuroscience : the official journal of the International Society for Developmental Neuroscience* 43, 70-77.

Fatemi, S.H., Folsom, T.D., Reutiman, T.J., and Lee, S. (2008). Expression of astrocytic markers aquaporin 4 and connexin 43 is altered in brains of subjects with autism. *Synapse* 62, 501-507.

Freeman, M.R. (2010). Specification and morphogenesis of astrocytes. *Science* 330, 774-778.

Frischknecht, R., Heine, M., Perrais, D., Seidenbecher, C.I., Choquet, D., and Gundelfinger, E.D. (2009). Brain extracellular matrix affects AMPA receptor lateral mobility and short-term synaptic plasticity. *Nature neuroscience* 12, 897-904.

Gallagher, A., and Hallahan, B. (2012). Fragile X-associated disorders: a clinical overview. *Journal of neurology* 259, 401-413.

Garcia-Marques, J., and Lopez-Mascaraque, L. (2013). Clonal identity determines astrocyte cortical heterogeneity. *Cerebral cortex* 23, 1463-1472.

Garrick, D., Samara, V., McDowell, T.L., Smith, A.J., Dobbie, L., Higgs, D.R., and Gibbons, R.J. (2004). A conserved truncated isoform of the ATR-X syndrome protein lacking the SWI/SNF-homology domain. *Gene* 326, 23-34.

Ge, W.P., Miyawaki, A., Gage, F.H., Jan, Y.N., and Jan, L.Y. (2012). Local generation of glia is a major astrocyte source in postnatal cortex. *Nature* 484, 376-380.

Gecz, J., Pollard, H., Consalez, G., Villard, L., Stayton, C., Millasseau, P., Khrestchatsky, M., and Fontes, M. (1994). Cloning and expression of the murine homologue of a putative human X-linked nuclear protein gene closely linked to PGK1 in Xq13.3. *Human molecular genetics* 3, 39-44.

Gibbons, R. (2006). Alpha thalassaemia-mental retardation, X linked. *Orphanet journal of rare diseases* 1, 15.

Gibbons, R.J., Picketts, D.J., Villard, L., and Higgs, D.R. (1995). Mutations in a putative global transcriptional regulator cause X-linked mental retardation with alpha-thalassaemia (ATR-X syndrome). *Cell* 80, 837-845.

Gibbons, R.J., Suthers, G.K., Wilkie, A.O., Buckle, V.J., and Higgs, D.R. (1992). X-linked alpha-thalassaemia/mental retardation (ATR-X) syndrome: localization to Xq12-q21.31 by X inactivation and linkage analysis. *American journal of human genetics* 51, 1136-1149.

Goldberg, A.D., Banaszynski, L.A., Noh, K.M., Lewis, P.W., Elsaesser, S.J., Stadler, S., Dewell, S., Law, M., Guo, X., Li, X., *et al.* (2010). Distinct factors control histone variant H3.3 localization at specific genomic regions. *Cell* 140, 678-691.

Gomes, D., Agasse, A., Thiebaud, P., Delrot, S., Geros, H., and Chaumont, F. (2009). Aquaporins are multifunctional water and solute transporters highly divergent in living organisms. *Biochimica et biophysica acta* 1788, 1213-1228.

Haj-Yasein, N.N., Jensen, V., Ostby, I., Omholt, S.W., Voipio, J., Kaila, K., Ottersen, O.P., Hvalby, O., and Nagelhus, E.A. (2012). Aquaporin-4 regulates extracellular space volume dynamics during high-frequency synaptic stimulation: a gene deletion study in mouse hippocampus. *Glia* 60, 867-874.

Haj-Yasein, N.N., Vindedal, G.F., Eilert-Olsen, M., Gundersen, G.A., Skare, O., Laake, P., Klungland, A., Thoren, A.E., Burkhardt, J.M., Ottersen, O.P., *et al.* (2011). Glial-conditional deletion of aquaporin-4 (Aqp4) reduces blood-brain water uptake and confers barrier function on perivascular astrocyte endfeet. *Proceedings of the National Academy of Sciences of the United States of America* 108, 17815-17820.

Hebert, J.M., and McConnell, S.K. (2000). Targeting of cre to the Foxg1 (BF-1) locus mediates loxP recombination in the telencephalon and other developing head structures. *Developmental biology* 222, 296-306.

Herculano-Houzel, S. (2014). The glia/neuron ratio: how it varies uniformly across brain structures and species and what that means for brain physiology and evolution. *Glia* 62, 1377-1391.

Higashimori, H., Morel, L., Huth, J., Lindemann, L., Dulla, C., Taylor, A., Freeman, M., and Yang, Y. (2013). Astroglial FMRP-dependent translational down-regulation of mGluR5 underlies glutamate transporter GLT1 dysregulation in the fragile X mouse. *Human molecular genetics* 22, 2041-2054.

Huh, M.S., Price O'Dea, T., Ouazia, D., McKay, B.C., Parise, G., Parks, R.J., Rudnicki, M.A., and Picketts, D.J. (2012). Compromised genomic integrity impedes muscle growth after Atrx inactivation. *The Journal of clinical investigation* 122, 4412-4423.

Ikeshima-Kataoka, H., Shen, J.S., Eto, Y., Saito, S., and Yuasa, S. (2008). Alteration of inflammatory cytokine production in the injured central nervous system of tenascin-deficient mice. *In vivo* 22, 409-413.

Irintchev, A., Rollenhagen, A., Troncoso, E., Kiss, J.Z., and Schachner, M. (2005). Structural and functional aberrations in the cerebral cortex of tenascin-C deficient mice. *Cerebral cortex* 15, 950-962.

Iwase, S., Xiang, B., Ghosh, S., Ren, T., Lewis, P.W., Cochrane, J.C., Allis, C.D., Picketts, D.J., Patel, D.J., Li, H., *et al.* (2011). ATRX ADD domain links an atypical histone methylation recognition mechanism to human mental-retardation syndrome. *Nature structural & molecular biology* 18, 769-776.

Jacobs, S., and Doering, L.C. (2010). Astrocytes prevent abnormal neuronal development in the fragile x mouse. *The Journal of neuroscience : the official journal of the Society for Neuroscience* 30, 4508-4514.

Jones, E.V., Bernardinelli, Y., Tse, Y.C., Chierzi, S., Wong, T.P., and Murai, K.K. (2011). Astrocytes control glutamate receptor levels at developing synapses through SPARC-beta-integrin interactions. *The Journal of neuroscience : the official journal of the Society for Neuroscience* 31, 4154-4165.

Jones, E.V., and Bouvier, D.S. (2014). Astrocyte-secreted matricellular proteins in CNS remodelling during development and disease. *Neural plasticity* 2014, 321209.

Kernohan, K.D., Jiang, Y., Tremblay, D.C., Bonvissuto, A.C., Eubanks, J.H., Mann, M.R., and Berube, N.G. (2010). ATRX partners with cohesin and MeCP2 and contributes to developmental silencing of imprinted genes in the brain. *Developmental cell* 18, 191-202.

Kernohan, K.D., Vernimmen, D., Gloor, G.B., and Berube, N.G. (2014). Analysis of neonatal brain lacking ATRX or MeCP2 reveals changes in nucleosome density, CTCF binding and chromatin looping. *Nucleic acids research* 42, 8356-8368.

Khakh, B.S., and Sofroniew, M.V. (2015). Diversity of astrocyte functions and phenotypes in neural circuits. *Nature neuroscience* 18, 942-952.

Kidd, S.A., Lachiewicz, A., Barbouth, D., Blitz, R.K., Delahunty, C., McBrien, D., Visootsak, J., and Berry-Kravis, E. (2014). Fragile X syndrome: a review of associated medical problems. *Pediatrics* 134, 995-1005.

Kucukdereli, H., Allen, N.J., Lee, A.T., Feng, A., Ozlu, M.I., Conatser, L.M., Chakraborty, C., Workman, G., Weaver, M., Sage, E.H., *et al.* (2011). Control of excitatory CNS synaptogenesis by astrocyte-secreted proteins Hevin and SPARC. *Proceedings of the National Academy of Sciences of the United States of America* 108, E440-449.

Laurence, J.A., and Fatemi, S.H. (2005). Glial fibrillary acidic protein is elevated in superior frontal, parietal and cerebellar cortices of autistic subjects. *Cerebellum* 4, 206-210.

Law, M.J., Lower, K.M., Voon, H.P., Hughes, J.R., Garrick, D., Viprakasit, V., Mitson, M., De Gobbi, M., Marra, M., Morris, A., *et al.* (2010). ATR-X syndrome protein targets tandem repeats and influences allele-specific expression in a size-dependent manner. *Cell* 143, 367-378.

Leung, J.W., Ghosal, G., Wang, W., Shen, X., Wang, J., Li, L., and Chen, J. (2013). Alpha thalassemia/mental retardation syndrome X-linked gene product ATRX is required for proper replication restart and cellular resistance to replication stress. *The Journal of biological chemistry* 288, 6342-6350.

Levy, M.A., Fernandes, A.D., Tremblay, D.C., Seah, C., and Berube, N.G. (2008). The SWI/SNF protein ATRX co-regulates pseudoautosomal genes that have translocated to autosomes in the mouse genome. *BMC genomics* 9, 468.

Levy, M.A., Kernohan, K.D., Jiang, Y., and Berube, N.G. (2015). ATRX promotes gene expression by facilitating transcriptional elongation through guanine-rich coding regions. *Human molecular genetics* 24, 1824-1835.

Lewis, J.D., Meehan, R.R., Henzel, W.J., Maurer-Fogy, I., Jeppesen, P., Klein, F., and Bird, A. (1992). Purification, sequence, and cellular localization of a novel chromosomal protein that binds to methylated DNA. *Cell* 69, 905-914.

Lioy, D.T., Garg, S.K., Monaghan, C.E., Raber, J., Foust, K.D., Kaspar, B.K., Hirrlinger, P.G., Kirchhoff, F., Bissonnette, J.M., Ballas, N., *et al.* (2011). A role for glia in the progression of Rett's syndrome. *Nature* 475, 497-500.

- Loyola, A., Bonaldi, T., Roche, D., Imhof, A., and Almouzni, G. (2006). PTMs on H3 variants before chromatin assembly potentiate their final epigenetic state. *Molecular cell* 24, 309-316.
- Maezawa, I., Swanberg, S., Harvey, D., LaSalle, J.M., and Jin, L.W. (2009). Rett syndrome astrocytes are abnormal and spread MeCP2 deficiency through gap junctions. *The Journal of neuroscience : the official journal of the Society for Neuroscience* 29, 5051-5061.
- Mauch, D.H., Nagler, K., Schumacher, S., Goritz, C., Muller, E.C., Otto, A., and Pfrieder, F.W. (2001). CNS synaptogenesis promoted by glia-derived cholesterol. *Science* 294, 1354-1357.
- McDowell, T.L., Gibbons, R.J., Sutherland, H., O'Rourke, D.M., Bickmore, W.A., Pombo, A., Turley, H., Gatter, K., Picketts, D.J., Buckle, V.J., *et al.* (1999). Localization of a putative transcriptional regulator (ATRX) at pericentromeric heterochromatin and the short arms of acrocentric chromosomes. *Proceedings of the National Academy of Sciences of the United States of America* 96, 13983-13988.
- Mori, T., Tanaka, K., Buffo, A., Wurst, W., Kuhn, R., and Gotz, M. (2006). Inducible gene deletion in astroglia and radial glia--a valuable tool for functional and lineage analysis. *Glia* 54, 21-34.
- Morte, B., and Bernal, J. (2014). Thyroid hormone action: astrocyte-neuron communication. *Frontiers in endocrinology* 5, 82.
- Muzumdar, M.D., Tasic, B., Miyamichi, K., Li, L., and Luo, L. (2007). A global double-fluorescent Cre reporter mouse. *Genesis* 45, 593-605.
- Nan, X., Hou, J., Maclean, A., Nasir, J., Lafuente, M.J., Shu, X., Kriaucionis, S., and Bird, A. (2007). Interaction between chromatin proteins MECP2 and ATRX is disrupted by mutations that cause inherited mental retardation. *Proceedings of the National Academy of Sciences of the United States of America* 104, 2709-2714.
- Nan, X., Ng, H.H., Johnson, C.A., Laherty, C.D., Turner, B.M., Eisenman, R.N., and Bird, A. (1998). Transcriptional repression by the methyl-CpG-binding protein MeCP2 involves a histone deacetylase complex. *Nature* 393, 386-389.
- Oberheim, N.A., Takano, T., Han, X., He, W., Lin, J.H., Wang, F., Xu, Q., Wyatt, J.D., Pilcher, W., Ojemann, J.G., *et al.* (2009). Uniquely hominid features of adult human astrocytes. *The Journal of neuroscience : the official journal of the Society for Neuroscience* 29, 3276-3287.
- Oberheim, N.A., Wang, X., Goldman, S., and Nedergaard, M. (2006). Astrocytic complexity distinguishes the human brain. *Trends in neurosciences* 29, 547-553.

Okabe, Y., Takahashi, T., Mitsumasu, C., Kosai, K., Tanaka, E., and Matsuishi, T. (2012). Alterations of gene expression and glutamate clearance in astrocytes derived from an MeCP2-null mouse model of Rett syndrome. *PloS one* 7, e35354.

Ong, C.T., and Corces, V.G. (2014). CTCF: an architectural protein bridging genome topology and function. *Nature reviews Genetics* 15, 234-246.

Pannasch, U., Freche, D., Dallerac, G., Ghezali, G., Escartin, C., Ezan, P., Cohen-Salmon, M., Benchenane, K., Abudara, V., Dufour, A., *et al.* (2014). Connexin 30 sets synaptic strength by controlling astroglial synapse invasion. *Nature neuroscience* 17, 549-558.

Pannasch, U., and Rouach, N. (2013). Emerging role for astroglial networks in information processing: from synapse to behavior. *Trends in neurosciences* 36, 405-417.

Picketts, D.J., Higgs, D.R., Bachoo, S., Blake, D.J., Quarrell, O.W., and Gibbons, R.J. (1996). ATRX encodes a novel member of the SNF2 family of proteins: mutations point to a common mechanism underlying the ATR-X syndrome. *Human molecular genetics* 5, 1899-1907.

Picketts, D.J., Tastan, A.O., Higgs, D.R., and Gibbons, R.J. (1998). Comparison of the human and murine ATRX gene identifies highly conserved, functionally important domains. *Mammalian genome : official journal of the International Mammalian Genome Society* 9, 400-403.

Powell, E.M., and Geller, H.M. (1999). Dissection of astrocyte-mediated cues in neuronal guidance and process extension. *Glia* 26, 73-83.

Preau, L., Fini, J.B., Morvan-Dubois, G., and Demeneix, B. (2015). Thyroid hormone signaling during early neurogenesis and its significance as a vulnerable window for endocrine disruption. *Biochimica et biophysica acta* 1849, 112-121.

Purcell, A.E., Jeon, O.H., Zimmerman, A.W., Blue, M.E., and Pevsner, J. (2001). Postmortem brain abnormalities of the glutamate neurotransmitter system in autism. *Neurology* 57, 1618-1628.

Pyka, M., Wetzel, C., Aguado, A., Geissler, M., Hatt, H., and Faissner, A. (2011). Chondroitin sulfate proteoglycans regulate astrocyte-dependent synaptogenesis and modulate synaptic activity in primary embryonic hippocampal neurons. *The European journal of neuroscience* 33, 2187-2202.

Quaegebeur, A., Lange, C., and Carmeliet, P. (2011). The neurovascular link in health and disease: molecular mechanisms and therapeutic implications. *Neuron* 71, 406-424.

Ritchie, K., Seah, C., Moulin, J., Isaac, C., Dick, F., and Berube, N.G. (2008). Loss of ATRX leads to chromosome cohesion and congression defects. *The Journal of cell biology* 180, 315-324.

Ritchie, K., Watson, L.A., Davidson, B., Jiang, Y., and Berube, N.G. (2014). ATRX is required for maintenance of the neuroprogenitor cell pool in the embryonic mouse brain. *Biology open* 3, 1158-1163.

Rossi, D. (2015). Astrocyte physiopathology: At the crossroads of intercellular networking, inflammation and cell death. *Progress in neurobiology* 130, 86-120.

Rothstein, J.D., Dykes-Hoberg, M., Pardo, C.A., Bristol, L.A., Jin, L., Kuncl, R.W., Kanai, Y., Hediger, M.A., Wang, Y., Schielke, J.P., *et al.* (1996). Knockout of glutamate transporters reveals a major role for astroglial transport in excitotoxicity and clearance of glutamate. *Neuron* 16, 675-686.

Seah, C., Levy, M.A., Jiang, Y., Mokhtarzada, S., Higgs, D.R., Gibbons, R.J., and Berube, N.G. (2008). Neuronal death resulting from targeted disruption of the Snf2 protein ATRX is mediated by p53. *The Journal of neuroscience : the official journal of the Society for Neuroscience* 28, 12570-12580.

Sicca, F., Imbrici, P., D'Adamo, M.C., Moro, F., Bonatti, F., Brovedani, P., Grottesi, A., Guerrini, R., Masi, G., Santorelli, F.M., *et al.* (2011). Autism with seizures and intellectual disability: possible causative role of gain-of-function of the inwardly-rectifying K⁺ channel Kir4.1. *Neurobiology of disease* 43, 239-247.

Slezak, M., Goritz, C., Niemiec, A., Frisen, J., Chambon, P., Metzger, D., and Pfrieder, F.W. (2007). Transgenic mice for conditional gene manipulation in astroglial cells. *Glia* 55, 1565-1576.

Sofroniew, M.V., and Vinters, H.V. (2010). Astrocytes: biology and pathology. *Acta neuropathologica* 119, 7-35.

Stayton, C.L., Dabovic, B., Gulisano, M., Gecz, J., Broccoli, V., Giovanazzi, S., Bossolasco, M., Monaco, L., Rastan, S., Boncinelli, E., *et al.* (1994). Cloning and characterization of a new human Xq13 gene, encoding a putative helicase. *Human molecular genetics* 3, 1957-1964.

Stevens, B., Allen, N.J., Vazquez, L.E., Howell, G.R., Christopherson, K.S., Nouri, N., Micheva, K.D., Mehalow, A.K., Huberman, A.D., Stafford, B., *et al.* (2007). The classical complement cascade mediates CNS synapse elimination. *Cell* 131, 1164-1178.

Tang, J., Wu, S., Liu, H., Stratt, R., Barak, O.G., Shiekhattar, R., Picketts, D.J., and Yang, X. (2004). A novel transcription regulatory complex containing death domain-associated protein and the ATR-X syndrome protein. *The Journal of biological chemistry* 279, 20369-20377.

Tsai, H.H., Li, H., Fuentealba, L.C., Molofsky, A.V., Taveira-Marques, R., Zhuang, H., Tenney, A., Murnen, A.T., Fancy, S.P., Merkle, F., *et al.* (2012). Regional astrocyte allocation regulates CNS synaptogenesis and repair. *Science* 337, 358-362.

Ullian, E.M., Sapperstein, S.K., Christopherson, K.S., and Barres, B.A. (2001). Control of synapse number by glia. *Science* 291, 657-661.

Verkerk, A.J., Pieretti, M., Sutcliffe, J.S., Fu, Y.H., Kuhl, D.P., Pizzuti, A., Reiner, O., Richards, S., Victoria, M.F., Zhang, F.P., *et al.* (1991). Identification of a gene (FMR-1) containing a CGG repeat coincident with a breakpoint cluster region exhibiting length variation in fragile X syndrome. *Cell* 65, 905-914.

Wada, T., Ban, H., Matsufuji, M., Okamoto, N., Enomoto, K., Kurosawa, K., and Aida, N. (2013). Neuroradiologic features in X-linked alpha-thalassemia/mental retardation syndrome. *AJNR American journal of neuroradiology* 34, 2034-2038.

Watson, L.A., Solomon, L.A., Li, J.R., Jiang, Y., Edwards, M., Shin-ya, K., Beier, F., and Berube, N.G. (2013). Atrx deficiency induces telomere dysfunction, endocrine defects, and reduced life span. *The Journal of clinical investigation* 123, 2049-2063.

Xue, Y., Gibbons, R., Yan, Z., Yang, D., McDowell, T.L., Sechi, S., Qin, J., Zhou, S., Higgs, D., and Wang, W. (2003). The ATRX syndrome protein forms a chromatin-remodeling complex with Daxx and localizes in promyelocytic leukemia nuclear bodies. *Proceedings of the National Academy of Sciences of the United States of America* 100, 10635-10640.

Yang, Y., Higashimori, H., and Morel, L. (2013). Developmental maturation of astrocytes and pathogenesis of neurodevelopmental disorders. *Journal of neurodevelopmental disorders* 5, 22.

Zamanian, J.L., Xu, L., Foo, L.C., Nouri, N., Zhou, L., Giffard, R.G., and Barres, B.A. (2012). Genomic analysis of reactive astrogliosis. *The Journal of neuroscience : the official journal of the Society for Neuroscience* 32, 6391-6410.

Zhang, Y., Chen, K., Sloan, S.A., Bennett, M.L., Scholze, A.R., O'Keefe, S., Phatnani, H.P., Guarnieri, P., Caneda, C., Ruderisch, N., *et al.* (2014). An RNA-sequencing transcriptome and splicing database of glia, neurons, and vascular cells of the cerebral cortex. *The Journal of neuroscience : the official journal of the Society for Neuroscience* 34, 11929-11947.

Appendix A – Ethics Approval

Submit - Animal Use Protocol - AUP Form

1. Investigator Contact Information

PI FULL NAME	Berube, Nathalie
AUP NUMBER	2008-041-02
AUP TYPE	
Primary Role	Principal Investigator
1. PI Full Name	Berube, Nathalie
2. Primary Institution & Department	Schulich School Of Medicine & Dentistry / Paediatrics
3. Office Location - Building & Room #	VRL A4-138
4. Weekday Phone #	55066
5. PI After-Hours Emergency Contact #	
6. Pager - Phone & Pager #	
7. Primary Email	
8. Other Email	
9. Lab Campus Location, if different from Q.3	Victoria Research Laboratory
10. Lab Phone #, if different from Q.4	55092

2. Protocol Title & Project Type

1. <i>Animal Use Protocol</i> Title
Investigating the role of chromatin proteins in brain development
2. Application Type, <i>Pick One</i>
Full Renewal
3. If 'Full Renewal' or 'Post-Pilot Full Protocol' provide Associated Previous Protocol Number
2008-041-01
4. If Post-Pilot Full Protocol or Full Renewal , Provide a 3 R'S PROGRESS REPORT SUMMARY that outlines progress relating to the REPLACEMENT of animals, REDUCTION of animal use numbers AND REFINEMENT of experimental technique. E.g. What did you previously learn that has resulted in a change in study design based upon application of the 3 R's. Link to CCAC's 3 R's Microsite for more information.
Replacement: For many of our experiments, we cannot use cell lines, as they do not completely replicate in vivo events. We can replace by establishing primary neuroprogenitor

Submit - Animal Use Protocol - AUP Form

<p>cultures, which mimic the neuronal differentiation process.</p> <p>Reduction: We are constantly striving to reduce our animal numbers by using each control/ ko pair for several different experiments. For example, we will use some pairs to investigate brain myelination or molecular events, but also keep the skeleton and other organs to investigate the systemic effects of ATRX loss of function.</p> <p>Refinement: For the CTCF project, we have now determined that inactivating CTCF with the Foxg1Cre driver line results in early complete loss of tissue. We are now concentrating our efforts on crossing with the NestinCre driver line, where we will investigate the histological and cellular outcomes of CTCF loss during embryogenesis. This refinement will translate into fewer mice used for this project.</p>
5. If Post-Pilot Full Protocol or Full Renewal , provide previous Protocol Year's animal use number.
161
6. Proposed Start Date (mm/dd/yy)
03/01/2012

Attachments List

File Spec	Description	Created
2008-041-02_7_0001_2008-041	2011 Annual Renewal	08/13/2014
Berube REN 03.01.11.doc		

3. Lay Summary & Glossary

<p>1. Using non-scientific language, please describe the project's purpose, expected benefit, and a brief summary of your work with the animal model(s). <i>Please be aware that in the event of communications with Western Media Relations and the PI is not available, this summary will be sent to Western Media Relations.</i></p>
<p>We are investigating the function of several proteins that regulate how DNA is structured and packaged in the nucleus. Mutations of several chromatin regulators cause developmental abnormalities, mental retardation syndromes, skeletal abnormalities, early aging phenotypes and cancer, emphasizing the importance of maintaining chromatin architecture in the developing brain. We are inactivating several proteins that cause cognitive deficits. ATRX, which is mutated in ATR-X</p>

Submit - Animal Use Protocol - AUP Form

mental retardation syndrome, MeCP2, which is mutated in the majority of Rett syndrome cases, and CTCF, a chromatin factor associated with ATRX. The experiments proposed under this protocol will help us delineate the cellular and molecular underpinnings of cognitive deficits and skeletal defects of the associated syndromes: ATR-X, Rett and Cornelia de Lange syndromes.

2. GLOSSARY OF TERMS - Identify each individual scientific term and abbreviation using *CAPITAL LETTERS*, and then briefly define each term to be referenced in any section of this protocol.

e.g. ALLELE - The genetic variant of a gene responsible for the different traits of certain characteristics and genetic diseases.

ATRX: Alpha Thalassemia mental Retardation syndrome, X-linked.

RTT: Rett syndrome

MeCP2: Methyl CpG binding protein 2

MUTATION; change in the nucleotide sequence

BrdU: Bromodeoxyuridine (BrdU) is a synthetic thymidine analog that gets incorporated into a cell's DNA when the cell is dividing (during the S-phase of the cell cycle).

Chromatin: the molecular structure comprised of DNA and its associated proteins

CTCF: CCCTC-binding factor, 11-zinc finger protein

4. CCAC Animal Procedural Outline

CCAC PROCEDURAL OVERVIEW - Use this field to convey in simple terms using approximately 40 words or less the nature of the procedures conducted on the animals.

Please use KEY WORDS provided through the above link.

The animals are used for fundamental and medical research purposes, and require the continuous maintenance of breeding colonies of genetically modified mice that model various human developmental syndromes. Mice are tagged, injected subcutaneously (BrdU or T4), or embryonic brain is used to establish primary cell cultures. In some cases, adult brain samples are taken for fixation and cryosectioning, or are frozen for subsequent isolation of RNA or protein. Sometimes the mice are euthanized to collect organs for DNA, RNA or protein extractions or are fixed and frozen for histological analyses. Blood samples will be taken for testing various metabolic parameters.

Academic Curriculum Vitae

Name: Haley McConkey

Education

Western University, London, On

Master's of Science

Sept 2013 –
Jan 2016

Specialization in Biochemistry and
Developmental Biology

Western University, London, On

Bachelor's of Medical Science

Sept 2009 –
April 2013

Honours Specialization in Clinical Biochemistry
Graduated with Distinction
Dean's Honour List 2009-2013

AWARDS

Ontario Graduate Scholarship, \$15000 - declined

Sept 2015 –
Aug 2016

Department of Paediatrics Graduate Studentship,
Western University, \$15000

Sept 2014 –
Aug 2015

Western Graduate Research Scholarship, *Western
University*, \$7500

Sept 2013 –
April 2015

Queen Elizabeth II Aiming for the Top Scholarship,
\$14000

Sept 2009 –
April 2013

Western Scholarship of Excellence, *Western
University*, \$2500

Sept 2009 –
April 2010

Publications and presentations

McConkey, H.N., Jiang, Y., and Bérubé, N.G. Poster: The Function of ATRX in Astrocytes, 2015. Presented at:

- Paediatrics Research Day, London, On – May 2015
- London Health Research Day, London, On, Top 80 Presenter – May 2015,
- Developmental Research Day, London, On – June 2015
- SONA, Hamilton – May 2015

McConkey, H.N., Jiang, Y., and Bérubé, N.G. Poster: The Function of ATRX in Astrocytes, 2014. Presented at:

- Canadian Conference on Epigenetics, Eh! London, On – June 2014
- Paediatrics Research Day, London, On – May 2014
- Developmental Biology Research Day, London, On – May 2014
- Department of Biochemistry Harold B. Stewart Memorial Lecture and Research Showcase, London, On – January 2014

McConkey, H.N., Xing, G., and Ling, H. Poster: The investigation of the interaction between ATAD5 and PCNA. Department of Biochemistry Harold B. Stewart Memorial Lecture and Research Showcase, London, On – January 2013

McConkey, H.N., Xing, G., and Ling, H. Oral Presentation: ATAD5/Elg1 interactions with PCNA. Presented at:

- Department of Biochemistry Final Undergraduate Thesis Presentation, Western University, London, On – April 2013
- Department of Biochemistry Introductory Undergraduate Thesis Presentation, Western University, London, On – October 2012